Universidad de La Laguna

Trabajo de Fin de Grado

Grado en Física

Optical Communications enhanced with automatic learning techniques with multispectral cameras as receivers

Alumno

Jorge González Díaz

Tutor

Julio Francisco Rufo Torres

Julio 2024

CONTENTS

1 Introduction

En el contexto actual, con un mundo completamente interconectado, es necesario el desarrollo de métodos más eficientes y seguros para transmitir información. En esta coyuntura, las comunicaciones ópticas por cámara, u OCC por sus siglas en inglés, se muestran como una alternativa novedosa que nos ayudará a resolver este problema. Este sistema utiliza fuentes de luz para emitir datos en forma de luz, que sea capaz de captarla el sensor óptico de una cámara y poder transmitir información en el proceso.

En este estudio se abordarán diferentes mecanismos para mejorar las comunicaciones ópticas a partir de la mejora del detalle de las imágenes tomadas por el sensor óptico de la cámara, utilizando la técnica de pansharpening para fusionar las bandas espectrales de la cámara con la banda pancromática. El objetivo es el de demostrar que a partir de esta técnica es posible mejorar las imágenes captadas por el sensor óptico y así hacer más efectiva y eficiente la comunicación inalámbrica por luz.

Currently, in a fully interconnected world, the necessity for the development of more efficient and secure methods of information transmission is a must. Optical Camera Communications (OCC) represents an innovative approach to addressing this issue. The system utilises light sources to emit information in the form of light and the camera sensor as a receiver, simultaneously transmitting information over several channels and employing multiple light sources, increasing the transmission volume.

In this study, we aim to enhance optical communications by improving the quality and detail of images captured by the camera sensor. This will facilitate more effective and efficient information transmission. The objective of this study is to demonstrate how the improvement of image quality through pansharpening can significantly enhance wireless optical communications.

2 Theoretical basis

En el marco teórico se abordan diferentes aspectos fundamentales que debemos saber para la mejora de imágenes. En primer lugar, conocer en detalle las OCC, cómo funcionan y qué características tienen, junto con sus principales ventajas y desventajas. Posteriormete, se explica los efectos que produce la variación de la temperatura sobre los diodos LED, generando un desplazamiento en el pico de emisión de estos en el espectro electromagnético. A continuación, se explica de forma detallada en qué consiste y para qué sirve la técnica de pansharpening y finalmente se desarrolla la base teórica de una transformada wavelet.

2.1 Optical Camera Communications (OCC)

2.1.1 OCC technology

Optical Camera Communication (OCC) is a communication technology based on the transmission and reception of information through different light sources, such as light-emitting diodes (LEDs) and receivers that could be optical cameras. The cameras in question could be of different types, with the receiver potentially being any electronic device that is commonly used in everyday life, such as mobile phones, tablets or computers. For this reason, this technology can be considered accessible to all public, as no previous investment is required to acquire it and it is able to work with existing resources, positioning it as a highly cost-effective technology in comparison to other, more traditional Visible Light Communication (VLC) systems. According to [1], the latest revision of the VLC standard, IEEE 802.15.7, includes OCC technology.

This OCC technology is mainly employed for low-speed communications, in contrast to other communication technologies such as WiFi, which allows the transmission of a higher amount of data within the same time interval. This is attributable to the limitations of the optical receiver, covering the camera and the fundamental light modulation techniques, which are not as sophisticated as those employed in other more traditional communication systems. Nevertheless, despite this limitation on the speed of information transmission, the cameras used in OCC have an inherent capacity for spatial multiplexing, which is a technique that allows multiple data signals to be transmitted simultaneously within the same communication channel. This allows the amount of information that can be emitted on the same channel in a certain time interval to be significantly increased.

Similarly, OCC cameras possess the ability to simultaneously capture multiple points of light, allowing them to discern and separate the information emitted by each individual LED in a series of flashing and emitting LEDs. To describe this system, we typically employ the MIMO (Multiple-Input Multiple-Output) scheme, which is a scheme commonly utilized in telecommunications in systems that use a specific number of transmitters and receivers to send and receive information in multiple signals simultaneously. In this manner, the application of the MIMO scheme to OCC technology, as exemplified by the aforementioned discussion, enables the transmission and reception of a significantly greater quantity of information within a given time interval. This is due to the fact that although each LED may possess a limited capacity for data transmission, the collective emission of several LEDs increases the total amount of information transmitted, thereby enhancing the performance of the communication system and optimising the utilisation of the available transmission space.

2.1.2 CMOS

It is common practice for OCC systems to utilise image sensors based on a technology known as CMOS (Complementary Metal Oxide Semiconductor). CMOS sensors are semiconductor

devices that capture light from emitters and convert it into electronic signals to create digital images. This sensor is widely used in industry, primarily due to its energy efficiency and its capacity to integrate a multitude of additional functions into the sensor itself, including image processing. The sensor is composed of a pixel array in which each pixel contains a photo diode that detects light from the LED. When illuminated by incident light, the photo diode generates a specific electrical charge, which is then amplified by a built-in transistor and converted into a voltage signal. This signal can then be analysed and processed. In this manner, the transistors of each pixel permit the signal of each pixel to be studied sequentially or simultaneously. The reading may be conducted row by row (rolling shutter) or the entire matrix at once (global shutter).

The principal attributes of CMOS sensors are very different, although it is possible to identify energy efficiency as one of the most significant. The reduced energy consumption of these sensors makes them suitable for use in portable devices. Concurrently, these sensors permit the reading and processing of information at a high rate, thereby enabling the capture of images in rapid succession or the recording of high-speed videos with a satisfactory degree of image quality and minimal noise.

However, CMOS also has a number of drawbacks, such as interference. When multiple channels are used, there can be interference between them when light of one wavelength is detected in another channel. For example, if light associated with red is detected by the channels associated with green or blue, this can cause errors in interpretation due to interference. This phenomenon is attributed to the inherent properties of the colour filters employed in these sensors, commonly referred to as cross-talk. Consequently, a series of compensation techniques are employed, comprising signal processing algorithms that are designed to rectify the cross-talk effects, thereby enhancing the differentiation of the signals captured by each channel and reducing the incidence of errors.

2.1.3 Multispectral and hyperspectral cameras

Although it is possible to utilise OCC in conventional cameras, it is considerably more effective and pertinent to employ multispectral and hyperspectral cameras. The number of bands that these cameras possess when receiving information is a defining characteristic. Conventional cameras typically have three bands, which are referred to as colour or RGB. In contrast, multispectral and hyperspectral cameras have a greater number of bands, and each of these bands can transmit information through OCC technology. This allows these cameras to transmit and receive a greater volume of information in the same time interval than cameras that only capture in RGB. To facilitate an appreciation of this comparison, an image in (2.1) is provided that illustrates the increase in bands and the impact this has on the image, depending on whether it was captured using one type of camera or another.

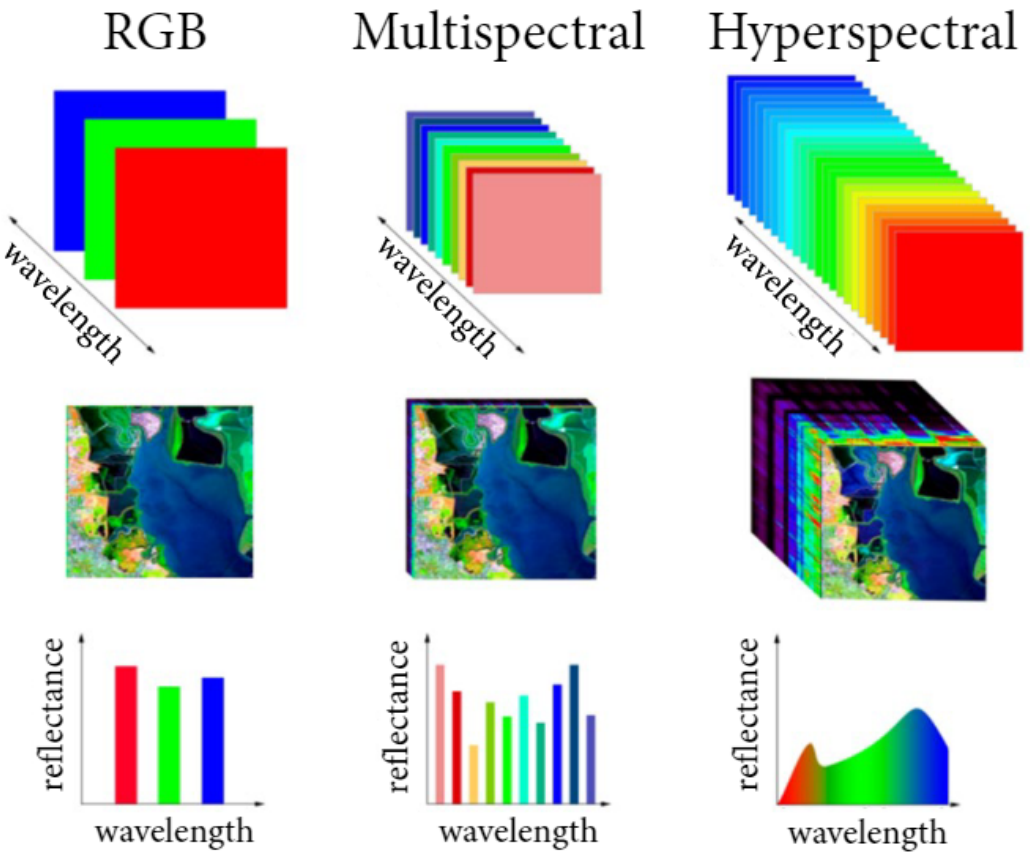

Figure 2.1: RGB, Multispectral and Hyperspectral camera's comparison.

Due to the higher level of information that MS and HS devices provide, these types of cameras have been usually employed in several sectors, such as remote sensing, healthcare industry, biotechnology, agriculture, *etcetera* [2, 3]. Initial studies utilized MS cameras for space-based imaging and remote sensing to analyze the environment since it provides more information than aerial photography. By capturing data across multiple spectral bands, these cameras enable the identification and characterization of specific materials, vegetation health, water quality, land-use classification, environmental monitoring, and archaeological sites. The ability to obtain comprehensive spectral data allows researchers and environmental agencies to study and monitor various ecosystems, track changes over time, and make informed decisions regarding land management, resource allocation, and conservation efforts [4, 5, 6]. One of the main applications in remote sensing is image classification. Hence, many studies applied classification techniques, such as unsupervised, semi-supervised, and supervised image classification (pixel-based techniques), and, more recently, due to the improvement of spatial resolution, obia to assign land cover classes to pixels [7, 8, 9].

Another common use of high spectral resolution cameras has been medical imaging to diagnose health issues. These cameras can capture spectral data beyond what is visible to the naked eye, providing detailed information about the biochemical composition and physiological properties of tissues and organs. With this information, medical professionals can improve the accuracy of diagnoses, monitor treatment effectiveness, and identify early markers of diseases. From early studies on magnetic resonance [10, 11] to new approaches in pathological diagnosis, non-contact detection, telepathology support systems, among others [12, 13, 14], clinical medicine has benefited from MS/HS imaging, especially as it enables noninvasive monitoring of human parameters.

Within the industrial sector, MS and HS cameras contribute to quality control, product inspection, process optimization, and military applications. These cameras can analyze the spectral signatures of materials, detecting defects or inconsistencies, and ensure adherence to specific standards or specifications. Industries such as food processing, pharmaceuticals, textiles, and electronics benefit from the ability to identify contaminants, assess product quality, and enhance production efficiency. By integrating MS and HS imaging technologies into industrial processes, companies can minimize waste, reduce costs, and improve overall product reliability and safety [15, 16, 17].

In agriculture, MS and HS cameras have revolutionized crop monitoring, precision farming, and yield optimization. By capturing spectral data from agricultural fields, these cameras allow farmers to assess crop health, detect nutrient deficiencies, identify disease or pest infestations, and determine optimal harvesting times [18, 19, 20].

Furthermore, for many years the field of MS/HS imaging has been bound to machine learning techniques in order to carry out classification analysis. In this regard, the last years have witnessed enormous growth in deep learning methods in different applications [21, 22, 23], improving classification accuracy and providing helpful characteristics for prediction.

Overall, the utilization of MS and HS cameras across these sectors demonstrates their significance in providing detailed information for a wide range of applications. However, to the best of my knowledge, no use of this kind of cameras has been performed in optical communication.

Therefore, the high level of spectral detail provided by MS cameras opens up new possibilities in the OCC field. In fact, the number of filters presented on MS/HS cameras allows a new approach for multiplexing signals of different wavelengths based on the spectral signature of the light source. Likewise, considering the temperature effects mentioned above, a high-spectral-resolution camera could be used to capture the variation of the LED's spectral emission. Hence, by inducing a controlled temperature to the LED, it would be possible to have the same light source with a different spectral signature. Consequently, this spectral variation could be used to implement several communication channels in an OCC link with a MS camera as a receiver.

2.1.4 Advantages and disadvantages of OCC

The principal distinguishing feature of the OCC is that, as it is VLC, i.e. it transmits data in the electromagnetic spectrum bands that the human eye is able to perceive, systems can be designed that verify visually and with great ease whether the transmission of information has been correctly produced. Similarly, the data can be modulated based on changes in colour or intensity in the LED, so that they are visible to the human eye and can be perceived. Alternatively, the information can be emitted by flickering the diode at high frequencies, so that the human eye is unable to observe these changes in light. This is a highly pertinent issue, as this technology would permit the transmission of information through flickering. Humans would be positioned in front of the light source, and its luminosity would be perceived as static. In contrast, the cameras would be able to observe the change in luminosity and receive that information. This would permit the creation of LEDs that could be perceived as either completely off or on. Such LEDs could be used in a variety of settings, including homes, vehicles, and hospitals. By monitoring the LEDs, it would be possible to identify potential issues with electrical systems, such as leaks of liquids or gases, or other problems that may arise over time. The utility of these systems in home maintenance and cultivation areas is evident, as they are capable of covering a considerable area while consuming minimal power. This makes them an economically viable option for installation and monitoring purposes.

However, as previously stated, for this VLC to occur, it is necessary to have a light emitter and a light receiver. Therefore, the system requires a direct wireless connection. If the receiver has opaque materials or objects that do not permit the light from the LED to pass through, it will not be able to receive this information. Consequently, if, for example, we wish to send information to a laptop via the light located in the ceiling of a room, and we take the computer to another room, this connection will be lost, and they will no longer have that information transmission channel. For this reason, in order to maintain this connection throughout a house, it would be necessary to connect all the lights in a house so that they transmit the same information. Conversely, it would be sufficient to cover the computer with any opaque object to disrupt the connection. This is why this system requires specific conditions that are not typically found in places such as a home. Bluetooth or WiFi technology allows for a wireless connection, but without the disadvantage of requiring a constant visual connection.

2.2 Effect of Temperature on LED

According to the authors of [24], the photons emitted by an LED present a wavelength that is related to the energy gap of the semiconductor substrate. It is also mention that the energy gap is affected by the p-n junction temperature, which is usually modelled using (2.1):

$$E_g = E_0 - \frac{\alpha T^2}{T + \beta} \tag{2.1}$$

where E_0 is the energy gap at 0K, T is temperature and α and β are semiconductor-dependent constants, which are empirically determined.

It is also a fact according to [25], that the energy gap in semiconductor materials decrease while the temperature increase. Hence, as wavelength is inversely proportional to this gap, the peak wavelength of the LED increases with temperature due to the Planck-Einstein equation (2.2) :

$$E_g = hf = \frac{hc}{\lambda} \tag{2.2}$$

where h is Planck´s constant, f is frequency, λ is wavelength and c is the speed of light in vacuum.

If we take $h = 6.626 \cdot 10^{-34} J \cdot s$ and $c = 2.998 \cdot 10^{8} m/s$ and multiply we get:

$$hc = 6.626 \cdot 10^{-34} J \cdot s \cdot 2.998 \cdot 10^{8} m/s = 1.99 \cdot 10^{-25} J \cdot m \tag{2.3}$$

The unit commonly used for small-scale energy, such as in electrons or photons, is the eV. To convert from eV to Joule, we need to know that $1eV = 1.602 \cdot 10^{-19} J$. So, if we rewrite the above equation in terms of eV:

$$hc = 1.99 \cdot 10^{-25} J \cdot m \cdot \frac{1eV}{1.602 \cdot 10^{-19} J} = 1.24 \cdot 10^{-6} eV \cdot m \tag{2.4}$$

If we put the wavelength in units of μm it would be as follows:

$$hc = 1.24 \cdot 10^{-6} eV \cdot m \cdot \frac{10^{6} \mu m}{1m} = 1.24 eV \cdot \mu m \tag{2.5}$$

The resulting equation, which is the most commonly used, relates the energy of a photon in eV to its wavelength in μm:

$$E(eV) = \frac{1.24}{\lambda(\mu m)} \tag{2.6}$$

Likewise, as expressed in [26], different investigations have studied the impact of temperature on photometric parameters. As an example of this, we have [27], where the optical parameters of LEDs from surface mount devices were determined under different thermal conditions, subsequently observing a red shift of the peak wavelength with increasing temperature. It was also observed that the spectral width, intensity and colour coordinate shifts of the devices changed as a dependence of temperature. In addition, as was done in [28], a number of

other relevant parameters were studied. In particular, both the luminous flux and the LED efficacy were studied under different conditions, showing that these parameters decrease as the junction temperature increases.

Also, it is important to note the high importance of the metallic content of the LED. The authors of [29] demonstrated that depending on the Indium content in InGaN alloys, the band gap may increase with temperature, specifically in green and blue LEDs. At the same time, in most cases, as the temperature increases, the spectral width increases and therefore the conversion efficiency decreases, as can be seen in [30].

As can be seen in articles [31], [32] and [33], it was observed that when LEDs were tested under different conditions of temperature and current through them, their lifetime, as well as their colour changes and luminous flux, were affected. Specifically, through these tests, an accelerated ageing of the LEDs was observed.

In this manner, by considering the preceding commentary and applying it to OCC technology, it is possible to increase or decrease the current that passes through an LED diode by varying the intensity of the light source and the resistance of the circuit. Consequently, the variation of the current would induce a variation in the temperature of the LED, which would cause a variation in the peak emission of this, shifting the peak at different points of the wavelength. To illustrate, if we consider a red LED and vary its current and therefore its temperature, it could change from a peak of 640nm to 680nm. If the optical receiver, or camera, has sufficient spectral bands to encompass both 640nm and 680nm, it will be able to differentiate between the two peaks. Consequently, if we designate the 640nm band as 0 and the 680nm band as 1, we could transmit information to the optical receiver just by deliberately varying the intensity of light transmitted through the light source. Consequently, the camera is capable of simultaneously transmitting information in each of the bands via pulses of light in each of them, and additionally, it is able to transmit a greater volume of information in the same time interval due to the temperature effect produced by the LED.

2.3 Pansharpening technique

Pansharpening is a technique commonly employed in image processing, particularly in the context of aerial and satellite imagery. It involves the combination of images of low spatial resolution, which we refer to as multispectral (MS), with images of higher spatial resolution, which we will refer to as panchromatic (PAN).

As outlined by [34], this technique involves the fusion of a multispectral (MS) image, which contains information about the different spectral bands that form it, but at low resolution, and a panchromatic (PAN) image, which contains data in a single band, but is wider and has a higher spatial resolution than the MS. The combination of a PAN and MS image results in an image with enhanced spatial resolution and spectral information. This technique is therefore highly relevant in improving the quality of images obtained during data acquisition. The final images produced have greater sharpness and detail, which notably improves their

visualisation. This in turn facilitates the interpretation of results and analysis, making it simpler and clearer. Conversely, the enhanced image quality and the ability to observe the image in colour facilitate more accurate classification, both supervised and unsupervised, thereby simplifying the detection of essential image characteristics for analysis in fields such as agriculture and cartography.

The main applications of pansharpening are predominantly associated with remote sensing and defence and security. On the one hand, it is a widely used technique in satellite imagery, facilitating the enhancement of image quality and detail for terrain analysis. This enables the study and monitoring of crops on agricultural land, as well as the examination of potential variations in soil moisture or irrigation practices, and the identification of potential threats to production, such as insect infestations or plant diseases. Furthermore, it is a valuable tool for the study of wooded areas, shallow lakes and rivers, and even urban areas, enabling the mapping of these regions and the tracking of their evolution over time. On the other hand, it is frequently employed in the domain of defence and security to obtain images for the purpose of surveillance and reconnaissance that could potentially compromise civil or state security.

At the same time, this technique has a number of methods that are applied in different areas, as each has its own characteristics. The most prominent methods are: the simple multiplication method, which consists of multiplying the MS image by the PAN image, so that a single image is obtained; the IHS (Intensity, Hue and Saturation) method, which consists of transforming the MS image to the IHS colour space, subsequently replacing the intensity component with the PAN image itself and finally taking the already modified image and transforming it back to the RGB space; and the Wavelet Transform method, which consists of decomposing the PAN and MS image, using the mathematical tool, the wavelet transform, in order to obtain the detail coefficients of the PAN image and the coefficients of the spectral bands of the MS image, with the aim of combining them and using them for the reconstruction of the final image.

Once one of the methods of the pansharpening technique has been applied, a number of filters are often employed in order to enhance the quality of the resulting images. This includes: the Smooth filter, which is used to improve the aesthetic appearance of an image by smoothing it and reducing its noise; the Edge Enhancement Filter and the Median Filter, which are typically employed when enhancing specific detail or features of an image. The median filter is typically employed for noise reduction, as it homogenises the resulting image. The wavelet transform is of particular relevance, as it forms the basis of the subsequent study and is capable of eliminating noise and enhancing different image details.

2.4 Wavelet Transform

The first thing to realise is that a wavelet is an oscillating mathematical function with a fixed duration. Unlike Fourier transforms, it is localised in time and frequency. The wavelet transform is a mathematical process in which the signal previously obtained in the space or time domain is transformed into a signal in the time-frequency domain. It is therefore a

mathematical tool that is mainly used to analyse signals at different resolution scales. It is particularly relevant to the processing of image and sound signals.

The main advantages and applications are, on the one hand, the localisation in time and frequency, since it provides us not only with information about the different frequencies present in a signal, but also with information about where these frequencies occur. Similarly, we highlight the usefulness of this mathematical tool in data compression, since when compressing images, a smaller number of coefficients is needed to efficiently represent the characteristics of the images. In signal processing, wavelets are very useful for identifying discontinuities, as well as for identifying transient characteristics of the signal or for eliminating the noise that appears in it.

The wavelet transform can be continuous (CWT) or discrete (DWT) as it is mention in [35].

2.4.1 Continuous Wavelet Transform (CWT)

The CWT is any wavelet transform that gives us all the points of a signal by sampling it continuously. We can see in (2.7) that the CWT can be described by an integral.

$$W_x(a,b) = |a|^{-1/2} \int_{-\infty}^{+\infty} f(t)\psi^*_{a,b}(\frac{t-b}{a})dt \tag{2.7}$$

Where $W_x(a,b)$ are the CWT coefficients, f(t) is the original signal, $\psi^*_{a,b}$ is the conjugate function complexity, and a and b are the scale and shift parameters.

2.4.2 Discrete Wavelet Transform (DWT)

The discrete wavelet transform (DWT) is a wavelet transform in which a discrete spectrum is taken by applying the sampling technique, which involves the use of a discrete scale and translation. As it does not take the entirety of the signal, but rather samples of it, this transform is more useful in computing environments when processing different signals. Concurrently, the DWT employs a series of filters to adapt the results to the most useful format for subsequent processing. In particular, low-pass and high-pass filters are typically employed. The low-pass filter smooths the signal by adjusting its points to the average between their neighbours, thereby reducing the large fluctuations between points. This process captures the general trends of the signal. In contrast, the high-pass filter amplifies the rapid fluctuations or details of the signal, thus facilitating their easier distinction.

if it is taken $a = 2^j$ and $b = k2^j$ where j is the decomposition level and k is the location index, we can rewrite 2.7 to get the equation that defines a discrete wavelet transform that is shown (2.8).

$$W_\psi(j,k) = 2^{-j/2} \int_{-\infty}^{+\infty} f(t)\psi^*_{j,k}(2^{-j}t - k)dt \tag{2.8}$$

Where if we take different discrete time series x_n, the DWT can be rewritten as follows in (2.9).

$$W_\psi(j,k) = 2^{-j/2} \sum_{n=0}^{N} \psi(2^{-j}t - k)x_n \tag{2.9}$$

Where x_n can be written as:

$$x_n = A(t) + \sum_{j=1}^{J} W_j(t) \tag{2.10}$$

Where $W_j(t)$ are the coefficients of details and A(t) is the aproximation at level J.

3 Methodology

En este apartado se especifica la descripción del procedimiento que se ha llevado a cabo a la hora de tomar los datos. Se explica por una parte el *software* y la forma en la que se obtuvo la información con la cámara y luego una explicación detallada del proceso de mejora de imágenes a partir de la técnica de pansharpening tanto para el *software* SNAP como para el de MatLab.

3.1 Description of procedures

Firstly, the LED spectral features were modified by inducing thermal changes in their p-n junction temperature. For this reason, and because no external sources were employed to heat the devices, the LEDs were powered at different currents for a period of time until they reached their thermal steady state. Second, behavior characteristics from the light sources were collected using various instrumentation equipment to characterize them and a MS camera to establish a communication link. Lastly, data were processed by applying several techniques to analyze them.

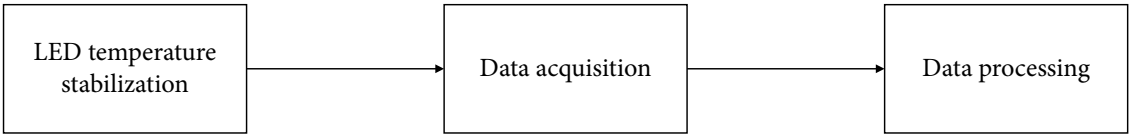

Figure 3.1: Common methods followed throughout this work.

The Colour Shades software was employed to capture images of the various bands that comprise the multispectral camera. Upon completion of a capture, the program returned a set of images, in which each of the colour bands were found separately. These included the panchromatic band with 1280x1024 pixels, an RGB image, and a series of images with different bands with 426x341 pixels. Additionally, a blog of notes was generated, in which all the relevant information pertaining to the capture and measurement was specified. This included the date and time, as well as the different bandwidths that each band of the camera had and its resolution. In figures (3.3, 3.4, 3.5 and 3.6), we can observe an exemplar of the data obtained from a single capture of a blue LED.

```
Image description

Exposure : 8.33 ms
Black Level : 116.00
Pixel Clock : 86.00 MHz
Frame Rate : 59.93 FPS

Model : CMS-C1-C-EVR1M-USB3
Camera SN : CMS22080267
FWHM (nm) : 75 58 42 34 31 28 27 25 15
Filter's centering (nm) : 430 470 510 550 579 620 662 705 0
Size image raw : 1280 x 1024
Size channel : 426 x 339
Coefficients channel normalizer : 1 1 1 1 1 1 1 1 1
Crosstalk correction : False
Coefficients white balance : 1 1 1

Output :


Image :
Index   |              Date                  |              Name
00001   |       2024.04.06_20:20:48.805      |              4_20240406_202048_805_00000
```

Figure 3.2: Blog of notes related to the information of the images.

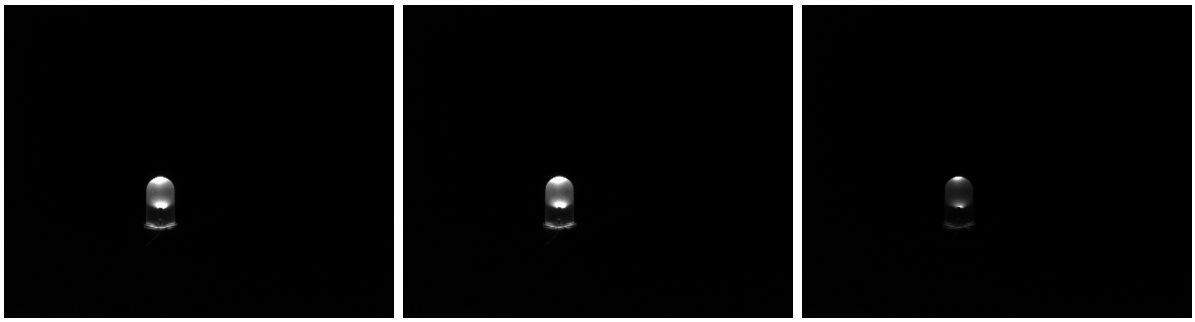

Figure 3.3: Bands: 0(430nm), 1(470nm) and 2(510nm).

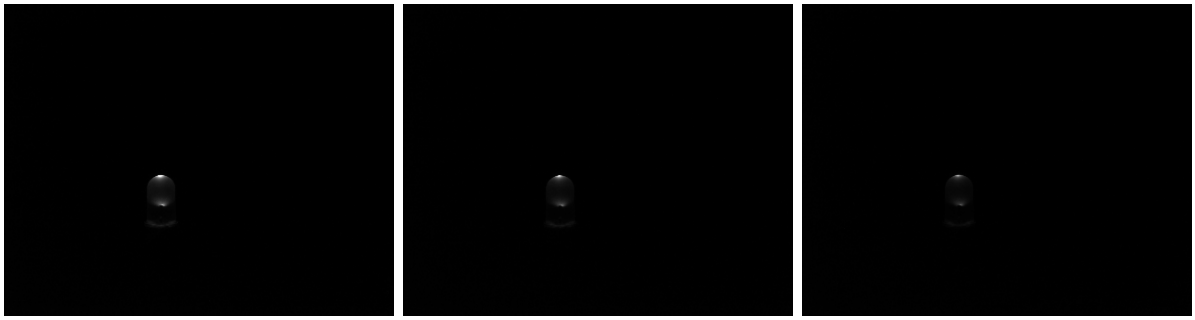

Figure 3.4: Bands: 3(550nm), 4(579nm) and 5(620nm).

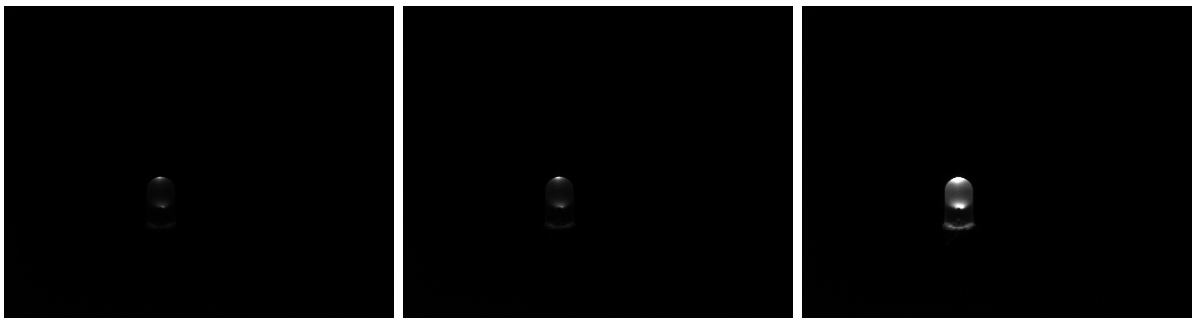

Figure 3.5: Bands: 6(662nm), 7(705nm) and 8(PAN).

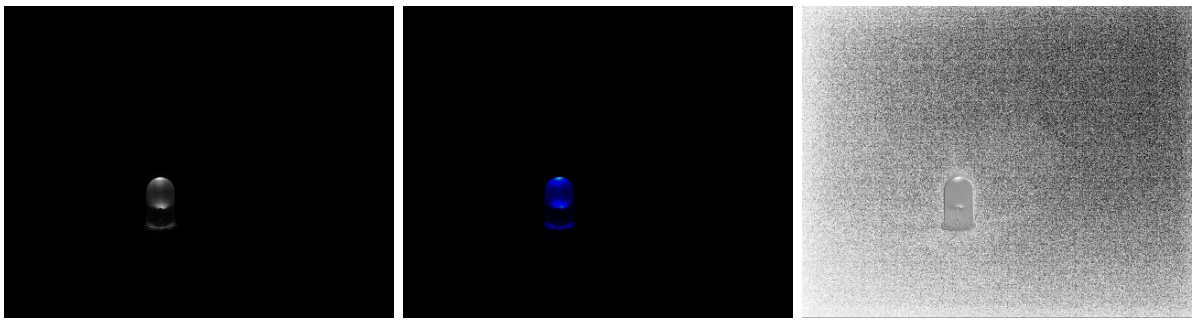

Figure 3.6: Panchromatic (PAN), Multispectral (MS) and Processed image.

With the data obtained, various tools were used to apply the pansharpening technique to the images, which was explained in the previous theoretical bases and which consists in merging the colour bands with the panchromatic band in order to obtain a coloured image with a higher resolution than the RGB image obtained during the data acquisition. The software used for this data processing was MatLab on the one hand and SNAP on the other. Both were used to compare which gave better results.

3.1.1 SNAP

The first step is to load the various images into the SNAP software. As we can see in the image below, we have a series of files on the left. Each of them represents, on the one hand, the PAN image, referred to as the raw image, and the MS image, referred to as the colour image, of each of the LEDs used for the study.

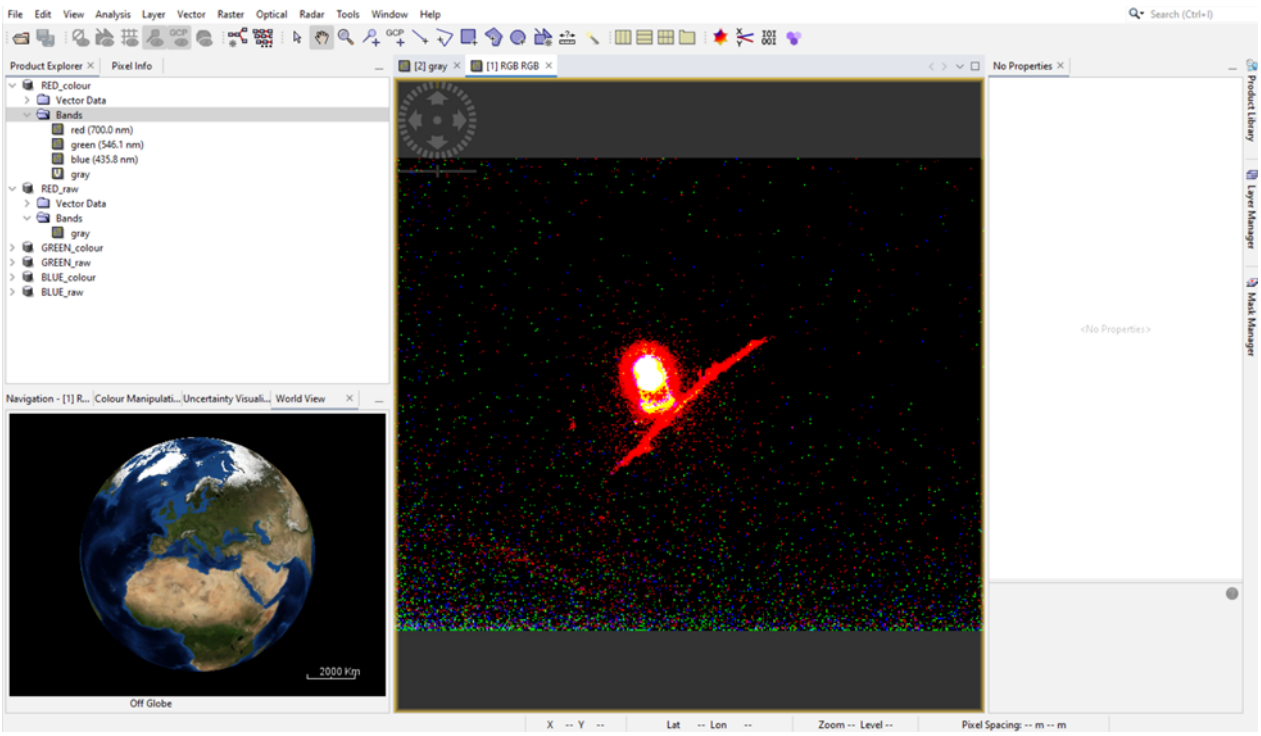

Figure 3.7: The SNAP software image was generated by inputting the images captured by the multispectral camera and the Color Shades software and merging the MS bands.

The following illustration presents a comparison between the MS image, which has a lower resolution, and the PAN image, which has a higher resolution, for each of the LEDs.

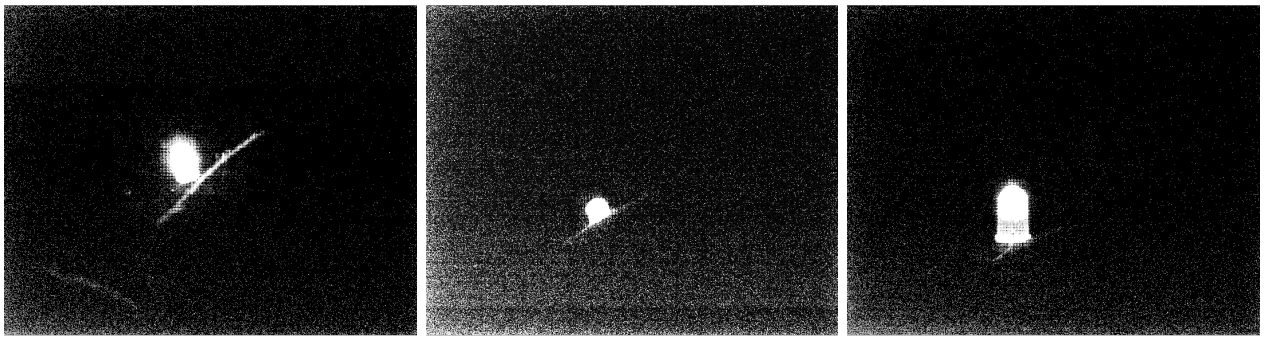

Figure 3.8: PAN images of Red, Green and Blue LEDs.

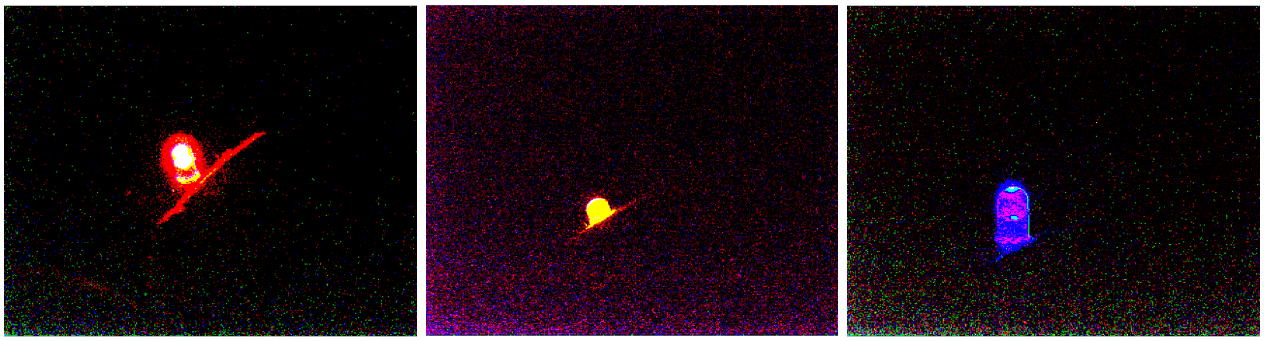

Figure 3.9: MS images of Red, Green and Blue LED.

Once we have the PAN and MS images, we need to apply the change in pixel size to the subsequent banding operation that will take place in SNAP, i.e. since the two images do not have the same number of pixels, we can increase or decrease the size of each pixel in one of the two images in order to have the same number in both. It is important to note that this does not increase or decrease the spatial resolution, as the information in the image remains the same. In this way, in the Raster tab, Geometric, select Resampling and choose the number of rows and columns that our final image will have. This time we have chosen to select the MS image and apply the upscaling. In the following figure we can see the resampling process of the MS of the red LED as an example.

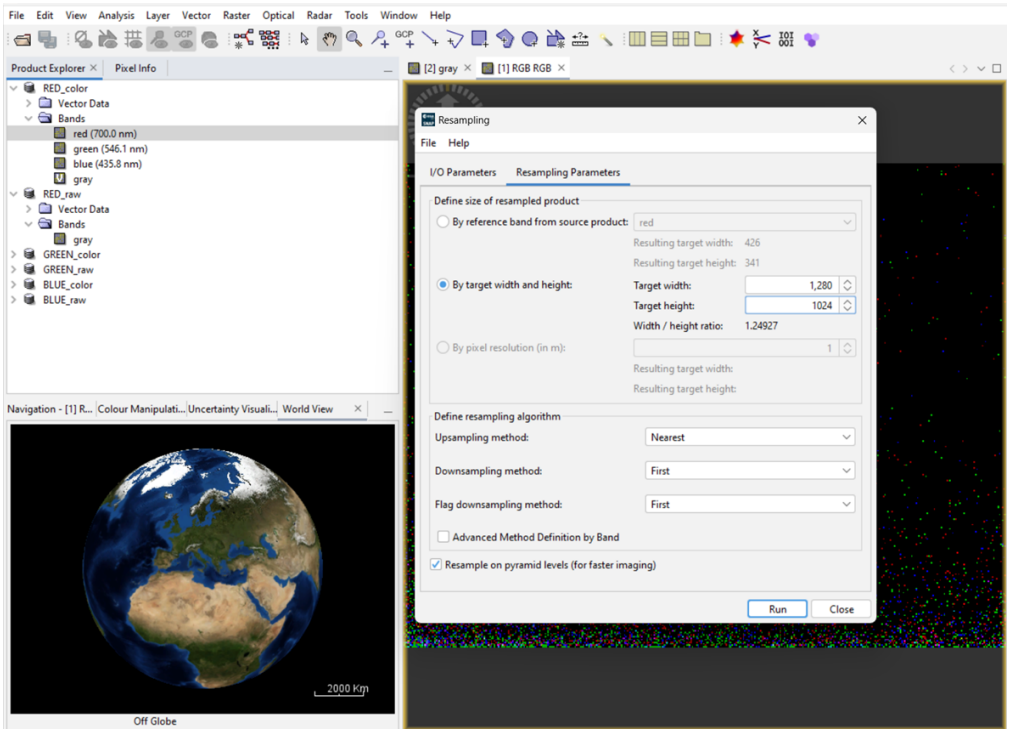

Figure 3.10: Image showing how the MS image is resized to match the size of the PAN.

Once we have resampled each of the MS images, it is now possible to perform operations on them. In this case, it is necessary to extract the details of each PAN image in order to merge them later with the colour bands. To do this, we use a low-pass filter whose purpose is to soften the contrasts of the image. It is important to note that applying a filter to an image, whatever it is, has a negative effect on the spatial resolution of the image, so it should only be used if it is necessary for what we need. So we select Raster, Filtered band as shown in (3.11).

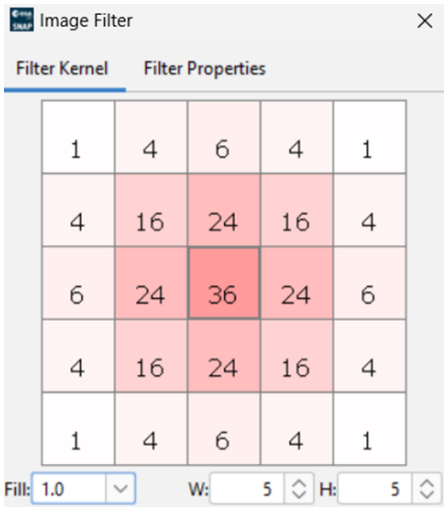

Figure 3.11: 5x5 low pass filter used in each PAN image.

Thus we obtained the three PAN images of the same size as the original pixel, but with half the spatial resolution. However, this is not enough to extract the detail from the PAN image, so we applied a low-pass filter again to make the image look as if the sensor had four times less resolution than the original, i.e. to resemble the resolution of the MS. Here (3.12) is the second filter used.

Figure 3.12: 9x9 low pass filter used in each PAN image.

Once the PAN image of each LED has been filtered twice, it can be clearly seen that the sharpness of these images is lower than in the original case, as can be seen in figures (3.13, 3.14). This is because the resolution of the double-filtered PAN is equal to the MS image of each LED.

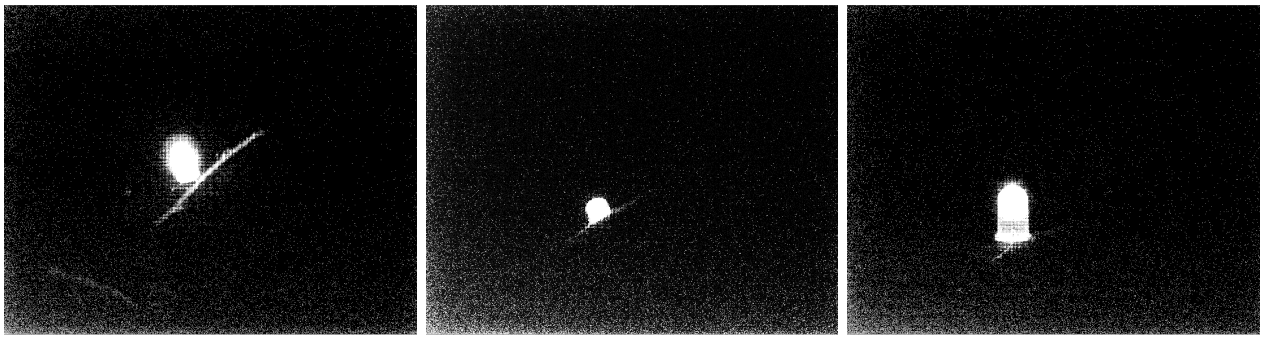

Figure 3.13: PAN images of Red, Green and Blue LEDs without filters.

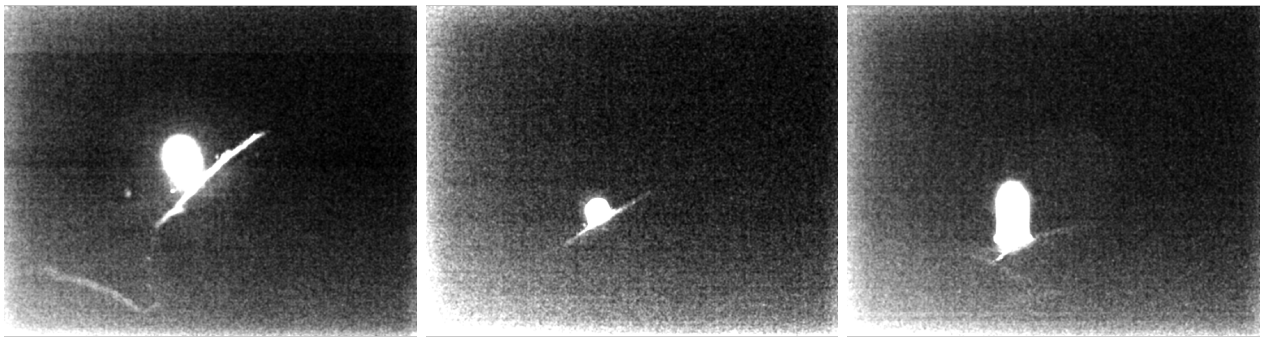

Figure 3.14: PAN images of Red, Green and Blue LEDs with both filters.

The pansharpening process continues with an operation that obtains the difference between the initial PAN band and the band with both filters applied. This is done in order to extract detail from the original PAN that the MS could not capture due to its low resolution. The band with both filters has four times less spatial resolution than the original PAN, and therefore the same resolution as the MS. This process allows us to obtain images of each of the LEDs with the additional detail provided by the original PAN. This is demonstrated in (3.15).

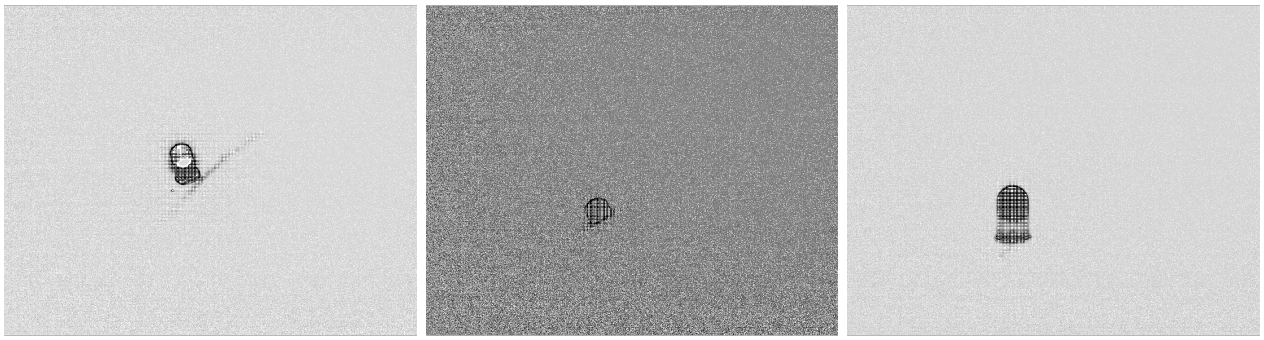

Figure 3.15: Red, Green and Blue LEDs only with its details.

Finally, the sum of the detail of each of the bands in the MS image of each of the LEDs is calculated. In order to achieve this, it is necessary to multiply the ratio between the standard deviation of the MS band being calculated and the initial PAN by the image containing the PAN detail. This is because both are different, and if this ratio is not included, there would be a certain error associated with each resulting image. The calculations that have been made for each band of each LED are the same as in (3.16).

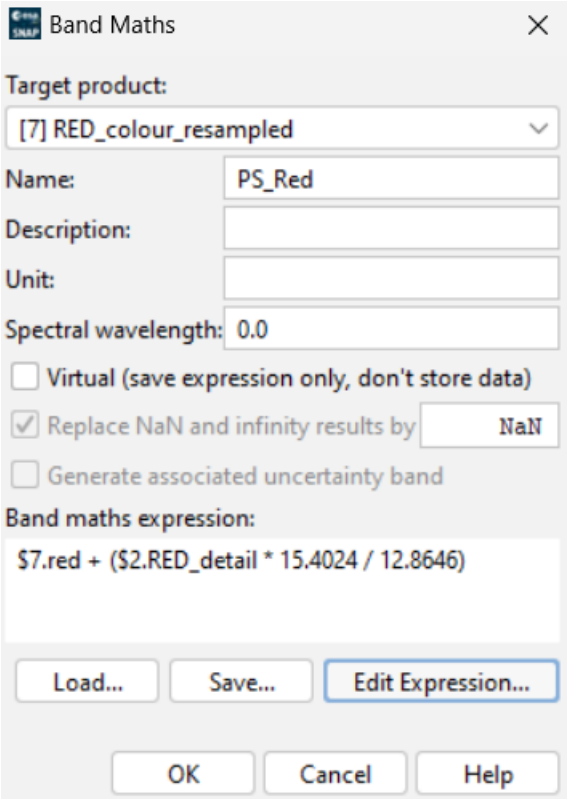

Figure 3.16: Illustration of an example for the calculation of one of the red LED bands.

Once the sum of the bands has been calculated, an image of each LED is produced, as can be seen in (3.17), which includes both the spatial information provided by the original PAN band and the spectral information provided by the MS band.

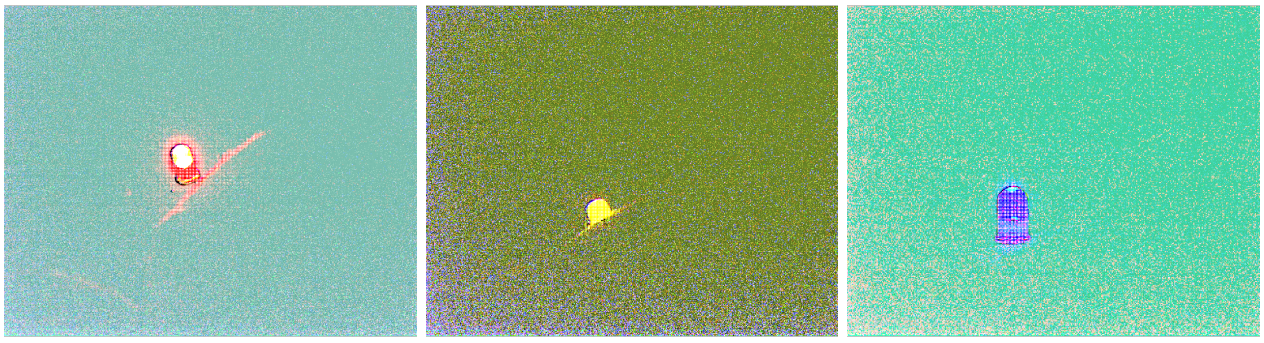

Figure 3.17: Red, Green and Blue LEDs once the pansharpening technique is completed.

3.1.2 MatLab

A pansharpening program is employed in the Matlab software with the objective of integrating the MS and PAN images, previously extracted from each LED diode, to enhance the resolution. Initially, the program initiates by reading both images and then PAN image is selected and resized to a dimension of 512 x 512 pixels. Similarly, the MS image is selected and resized to a size of 256x256 pixels.

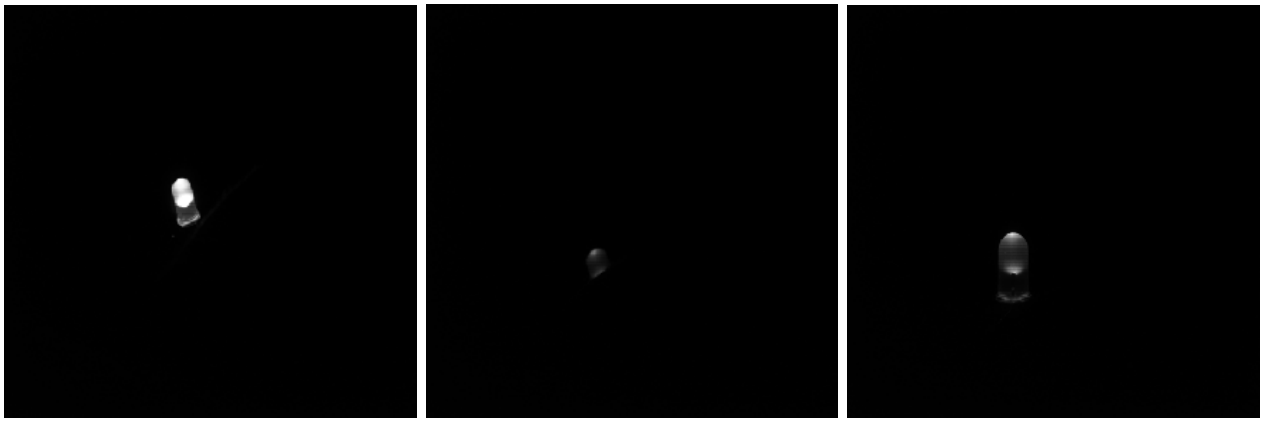

Figure 3.18: PAN images of Red, Green and Blue LEDs.

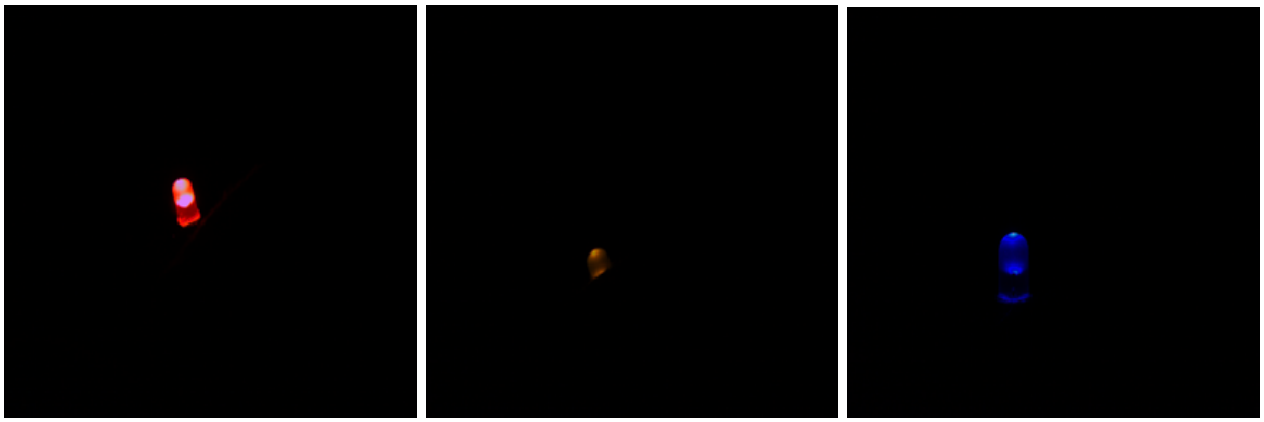

Figure 3.19: MS images of Red, Green and Blue LEDs.

Then, the MS image is resized to 512x512 pixels in order to match the size of the PAN. Subsequently, an Undecimated Discrete Wavelet Transform (USWT) is performed on both images utilising the wavelet sym4, which decomposes each image into a series of approximation and detail coefficients in different directions. An injection model is then calculated. In order to achieve this, the covariance between the PAN and MS image approximation coefficients is obtained, and a gain factor is calculated for each band of the MS image. This allows the determination of how the coefficients of both images will match in the fusion or pansharpening process. The post-USWT images are presented in **Appendix A**.

Following this, the images are fused by combining the approximation coefficients of the MS image and the PAN coefficients using the injection model. Thereafter, the detail coefficients between images are summed in each direction, and an inverse wavelet transform is performed, which reconstructs the fused image from the combined coefficients. Also in **Appendix A** we can see post-USWT PAN image and the decoded one. Finally, the fused and enhanced image, the original PAN and the original MS are presented for comparison. This allows the effectiveness of the image fusion technique to be evaluated in terms of image quality. The results for each of the LEDs are shown separately.

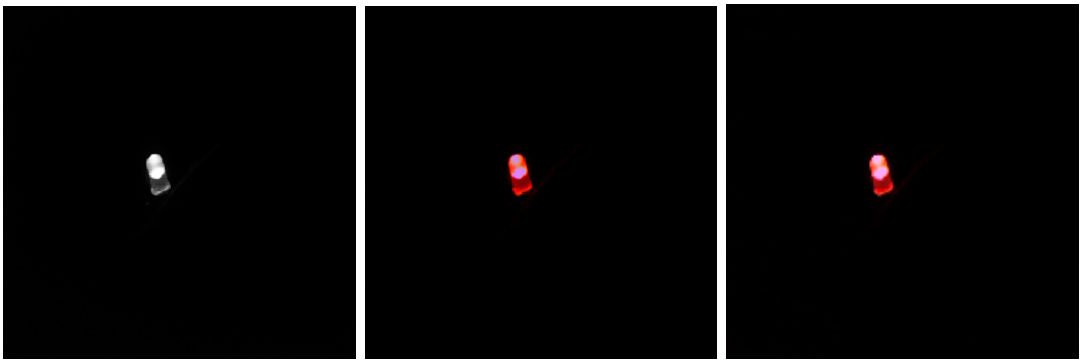

Figure 3.20: original PAN, original MS and enhanced images of Red LED.

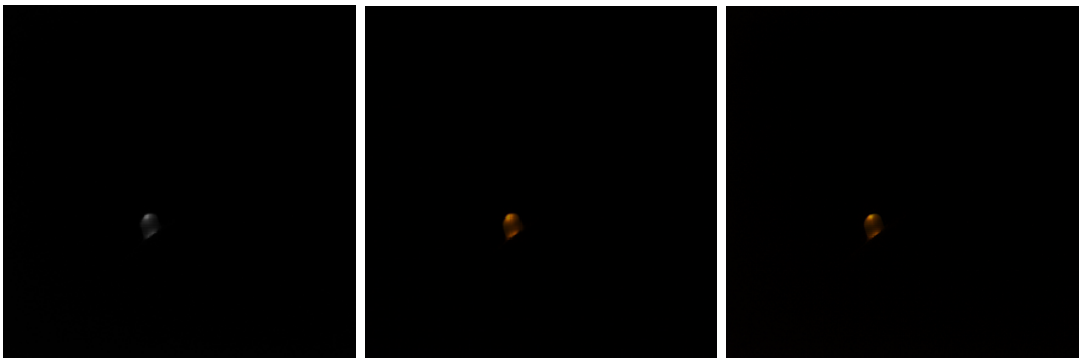

Figure 3.21: original PAN, original MS and enhanced images of Green LED.

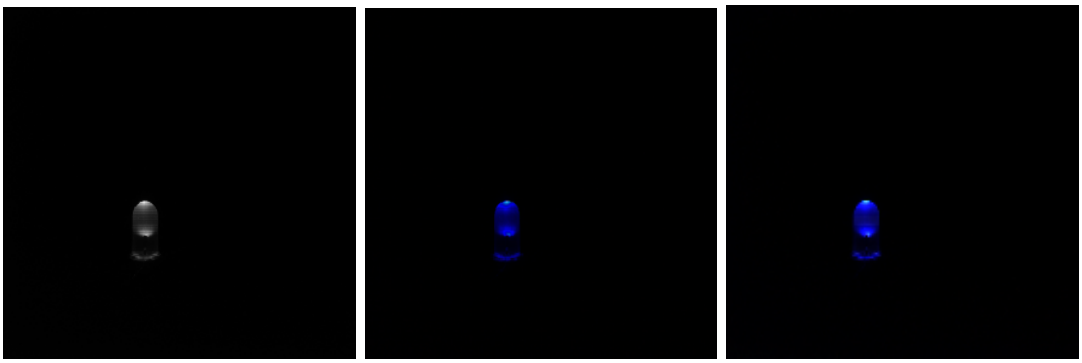

Figure 3.22: original PAN, original MS and enhanced images of Blue LED.

As can be observed, the enhanced final image represents a notable enhancement over the initial PAN image, particularly in terms of brightness and, most notably, in the red and blue LEDs. This evidence thus corroborates the assertion that the program has been able to optimise the image through the utilisation of this technique.

4 Implementation

En esta sección se detalla la implementación de la metodología comentada anteriormente. Se muestra por una parte el equipo empleado para la toma de medidas, así como el *software* de Color Shades Labs que utiliza la cámara para obtener y procesar las imágenes. A su vez, se obtienen las diferentes imágenes de cada uno de los diodos bajo los diferentes niveles de brillo a los que han sido sometidos.

4.1 Experimental Setup

A number of tools were needed to obtain the data. These included a multispectral camera, in this case a CMS series camera from Silios Technology, which has 8 bands in the visible and near-infrared range and a panchromatic band whose resolution is much higher than the rest. In turn, an Arduino to connect the different LEDs of red, green and blue colours and a computer to connect both and collect the information from the installed Color Shades Lab software.

In order to obtain the data, we proceeded as follows. To avoid systematic errors in the measurement, it was necessary to have an absence of light other than that of the LED itself. Therefore, it was decided to obtain the data in a closed room, where the external light was reduced as much as possible. In this way, the multispectral camera would take the measurements only with the light emitted by the LED. The system was therefore positioned on the floor, with the multispectral camera oriented directly towards the LED and connected to a laptop computer with its back facing the camera. This configuration prevented the camera from detecting the light emitted by the computer screen. The laptop was then connected to both the multispectral camera and the Arduino, which housed the LED. This setup enabled the use of the software Color Shades, developed by Silios Technology, to monitor the camera's various bands at all times. The following images illustrate the configuration of the measurement apparatus in a lit room, allowing for accurate observation.

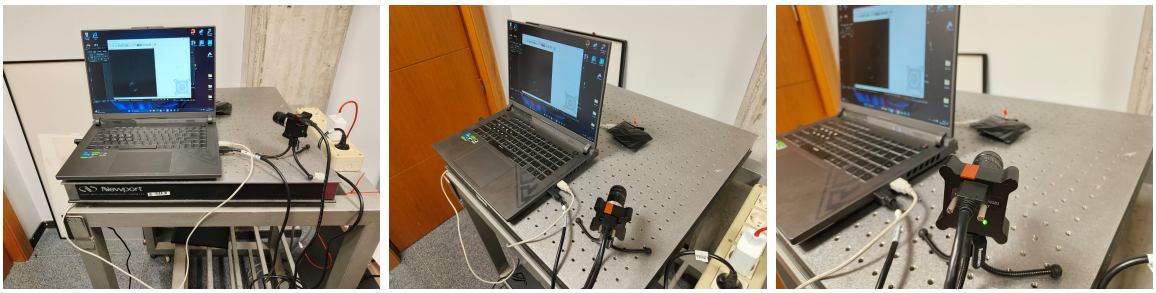

Figure 4.1: Images from different angles of the data collection setup. They were taken with external light for better viewing.

Figure 4.2: Screenshot of the Color Shades Labs software once the multispectral camera is connected and the blue LED is set.

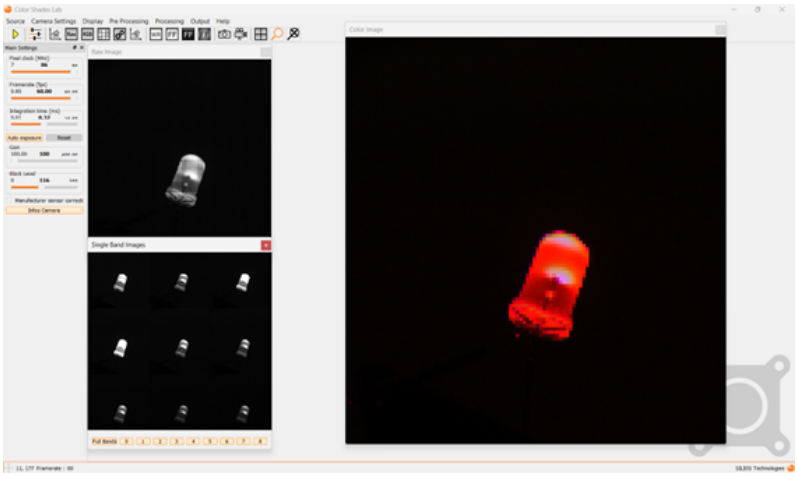

Figure 4.3: Picture from the Color Shades Labs software of the zoomed red LED together with its panchromatic band, all its separate bands and an RGB image from the program.

4.2 Shifts in peak wavelength from brightness variations

In this part of the study, the methodology previously described is modified. Instead of using stationary current conditions, as previously described, a variable current is employed. This results in a variation in the brightness of each light source.

In this procedure, we employed the Arduino's native software system to assess the impact of varying LED brightness on image quality. The hypothesis was that an increase in current passing through the LED would result in an increase in both its brightness and temperature, which would affect its emission peak to shift to another wavelength. This was based on the **Theoretical basis** presented in *Effect of Temperature on LED*. If the wavelength shift is sufficiently large and the camera has sufficient precision and the requisite number of bands in the electromagnetic spectrum, it will be able to capture the wavelength shift. The method for capturing this phenomenon would be to observe which band exhibits the greatest luminosity. To illustrate, consider a red LED with a specific brightness level. If the maximum luminosity is observed in band 5, but at a different brightness level, it can be concluded that the camera is capable of differentiating this displacement from the emission peak. Consequently, it is evident that the greater the number of bands in the optical receiver, namely in our multispectral camera, the greater the camera's capacity to discern this shift.

This phenomenon can be observed in Figures for Red (4.4,4.5,4.6), for Green (4.7,4.8,4.9) and for Blue (4.10,4.11,4.12), which illustrates how the various bands associated with a specific colour of each LED change at different intensities. This allows us to ascertain whether the camera has been able to capture the shift in wavelength.

Figure 4.4: Images of Red LED in Channels: 4, 5 and 6, with level 10 of brightness.

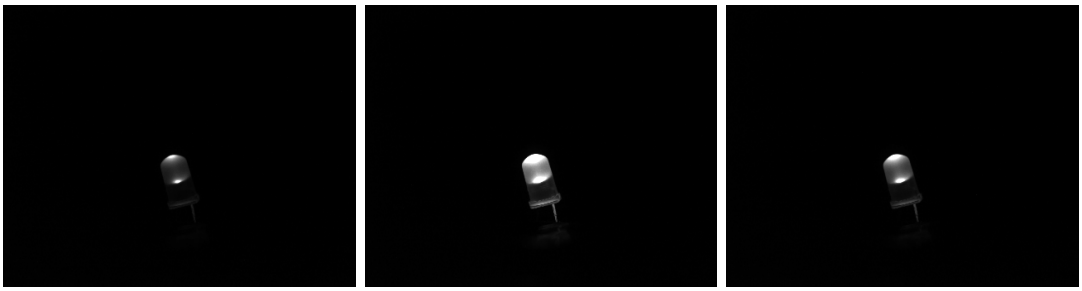

Figure 4.5: Images of Red LED in Channels: 4, 5 and 6, with level 50 of brightness.

Figure 4.6: Images of Red LED in Channels: 4, 5 and 6, with level 200 of brightness.

Figure 4.7: Images of Green LED in Channels: 3, 4 and 5, with level 10 of brightness.

Figure 4.8: Images of Green LED in Channels: 3, 4 and 5, with level 50 of brightness.

Figure 4.9: Images of Green LED in Channels: 3, 4 and 5, with level 200 of brightness.

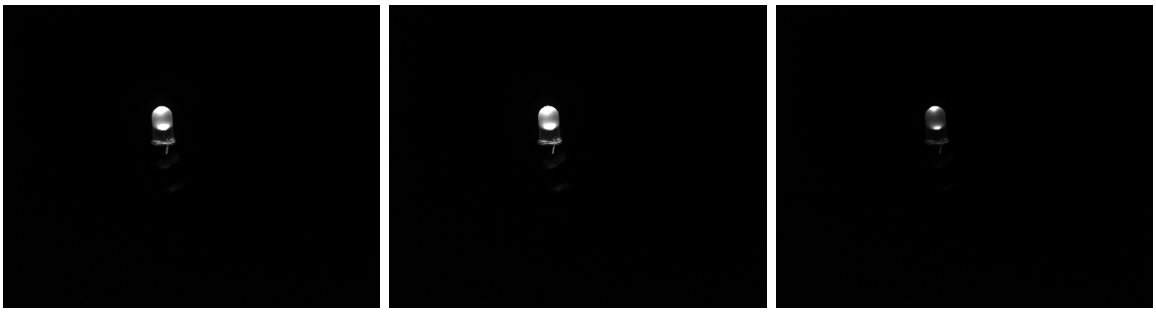

Figure 4.10: Images of Blue LED in Channels: 0, 1 and 2, with level 10 of brightness.

Figure 4.11: Images of Blue LED in Channels: 0, 1 and 2, with level 50 of brightness.

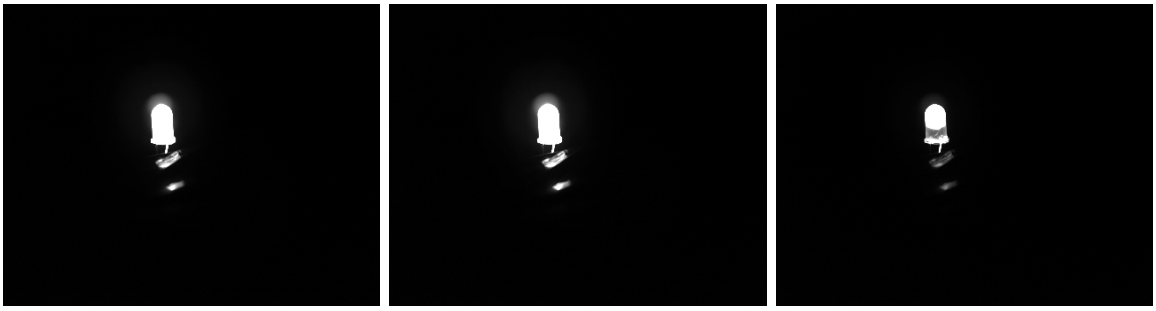

Figure 4.12: Images of Blue LED in Channels: 0, 1 and 2, with level 200 of brightness.

As illustrated in the accompanying images, the emission peak for a brightness of 10 in the case of the red LED is observed to be in band 5. However, as the current increases and the LED's temperature and brightness rise, this peak shifts, such that at a brightness of 200, band 5 and band 6 capture practically the same intensity. This phenomenon is not observed for a brightness of 50, where it can be seen that despite the increase in brightness, band 5 continues to be the predominant of the three. On the other hand, when examining the case of the green LED, its luminosity is so low in comparison to the red LED that the only discernible change is an increase in brightness, rather than a shift between bands. This suggests that in order to observe the shift, it would be necessary to use a brighter diode, increase the brightness even further, or decrease the series resistance in order to increase the current. Similarly, as observed in the case of the red LED, the blue LED also exhibits a shift in emission peak wavelength as the brightness increases. Initially, the emission peak is observed in channel 0, but as the brightness increases, it shifts to channel 1, producing the shift in wavelength in the emission peak that was proposed at the beginning.

5 Results

En la sección de resultados se discuten las imágenes finales de los distintos diodos LED una vez aplicada la técnica de pansharpening, a cada una de ellas a partir del SNAP y luego MatLab, en cada uno de los niveles de brillo seleccionados, que se han denotado como 10, 50 y 200. Se observan claras diferencias entre ambos métodos, ya que el fondo es diferente en cada uno, así como el ruido que se observa, y se aprecian colores distintos en su interior y silueta. Se abordará el razonamiento de estos factores, así como los reflejos que se forman en la parte inferior de los diodos en ciertas imágenes finales obtenidas. Con ello, se hará una valoración sobre los aspectos a destacar de cada una de las técnicas, y si ambos métodos nos proporcionan resultados satisfactorios con respecto a los objetivos que se habían propuesto en un inicio en el estudio, que es la mejora en la resolución de la imagen final a partir de la fusión de la banda multiespectral y la pancromática.

The use of the pansharpening technique through the SNAP software and MatLab resulted in a notable improvement in the images obtained for the case in which the current passing through the light source was constant. This can be observed in the section **Methodology**. For this reason, we have attempted to enhance the images of each LED by varying its luminosity. The maximum limit for each source was 255, but these ranges were selected for the purpose of studying the displacement of the emission peak in each case. Nevertheless, we elected to enhance each image at each brightness level to ascertain whether the image quality was demonstrably affected. The potential for low brightness to result in insufficient clarity and the possibility of excessive brightness causing glare or interference, which could affect the final image, led to the study of the colour images of each image for comparison.

The images of each LED at varying brightness levels, as seen here (5.1, 5.2, 5.3), were obtained using the SNAP software.

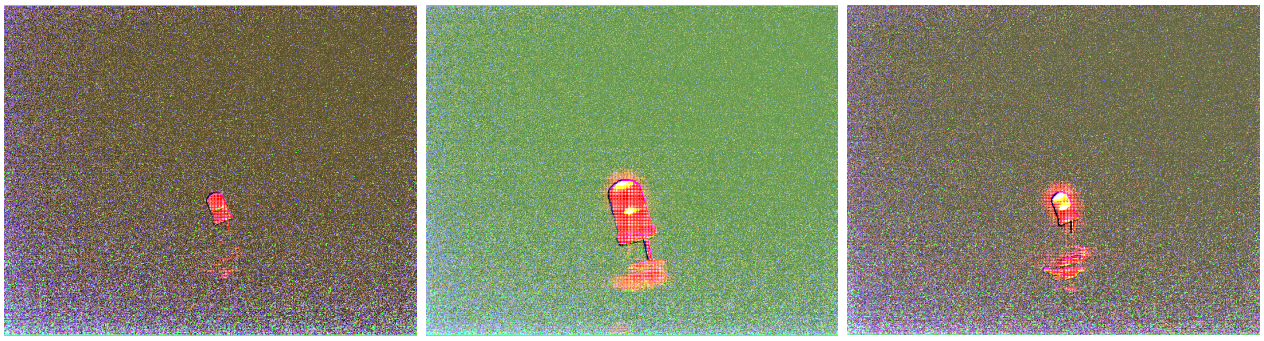

Figure 5.1: Images of Red LED in SNAP with levels 10, 50 and 200 of brightness.

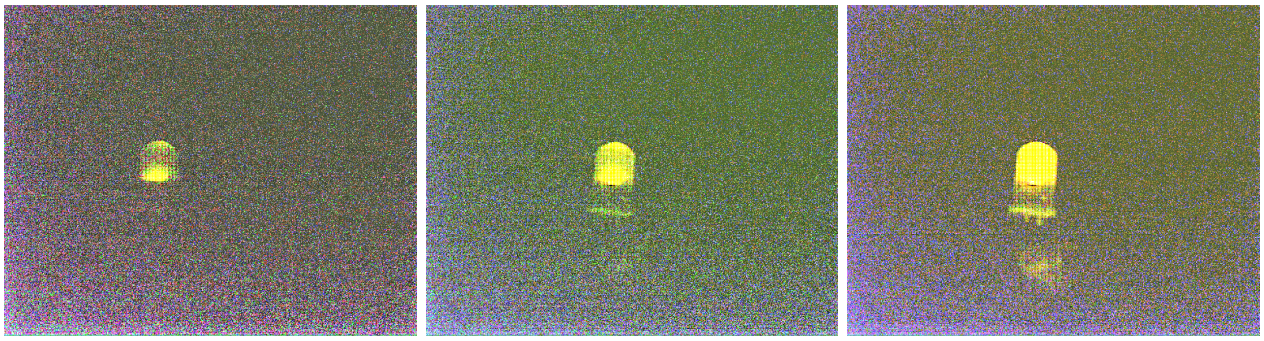

Figure 5.2: Images of Green LED in SNAP with levels 10, 50 and 200 of brightness.

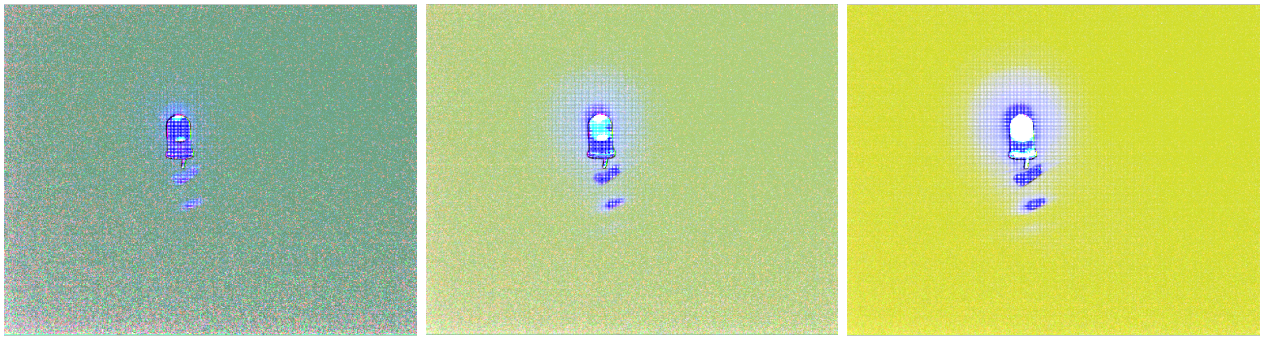

Figure 5.3: Images of Blue LED in SNAP with levels 10, 50 and 200 of brightness.

A comparison of the images reveals significant differences when they are considered in the context of the wider study. It is evident that the background of all images is of a markedly different colour to the black observed in the others. This discrepancy is likely attributable to the fact that the SNAP software is primarily employed for remote sensing applications. Consequently, it is plausible that the system is not optimised for the acquisition of images of this nature, which typically exhibit a higher spatial resolution and utilise distinct sensors compared to the multispectral camera utilised. For this reason, it is possible that the software itself employs a distinct methodology for processing images, which may result in the distortion of images that deviate from the typical characteristics of the system.

In contrast, as the brightness of the three LEDs is increased, a spot of the same colour can be observed at the lower part of them, which also grows. This phenomenon can be attributed to the formation of different reflections at the base of it due to the increase in brightness. As the Arduino was employed to transmit light commands to the LED, a number of red lights were present that could potentially lead to erroneous results. Hence, it was deemed necessary to cover these lights with an opaque black object. However, if the brightness of the source was

increased to an excessive degree, this resulted in the reflection that can be observed. In the specific case of the red source, it can be clearly seen that for a brightness of 10, its reflection is far away from itself and is very faint. In contrast, for the cases in which the brightness is set at 50 and 200, it can be seen that the reflection is not only touching part of the LED, but is much brighter and is perceived as larger. In the event that these images are to be utilised for the purpose of transmitting information via OCC, other materials must be employed in order to minimise the occurrence of reflections. Furthermore, the software utilised should be equipped with the requisite tools to enable the differentiation of these reflections from the light source, thus reducing errors in transmission.

A similar observation can be made in the different brightness series of each diode, whereby as the brightness increases, the sources can be better differentiated from the background. This is a logical consequence of the fact that as a source increases the amount of light it emits, the residual illumination tends to be less affected, resulting in a final image that carries less noise. This is exemplified by the green LED, where at brightness 10, only a portion of the diode is visible, and the surrounding noise is so substantial that an automated classification system would likely find it more challenging to differentiate the source from the noise. Consequently, optical communication at this brightness would be exceedingly complex, as there would be a multitude of errors due to the noise, rendering the transmission of information a significant challenge. However, when the brightness is increased to 50, the definition and detail of the diode in the image begin to improve. The colouration of the diode is markedly distinct from that of the background, and the entire silhouette of the diode is clearly discernible. Upon examination of the diode at a brightness of 200, it becomes evident that the colours within the LED and those surrounding it are entirely distinct, allowing for the precise identification of the source of background noise.

In the case of the blue LED, it can be observed that the background exhibits the greatest change in colour as the brightness is increased. At a brightness of 10, the colour of the background is similar to that of the source, making it challenging to distinguish it from the background itself. This can lead to classification errors in the system. However, at a brightness of 50 and particularly at a brightness of 200, it is observed that the diode is significantly different from the background, such that it could be classified automatically without errors.

It is worth noting that the colour of the background in this type of image is less significant than the distinction between it and the light source. In the case of using automatic image classification systems to transmit information, it is not necessary for the background to be black or of another colour; rather, it must be markedly different from that of the diode itself. This ensures that the automatic classification does not result in errors when studying the region of interest, which is located within the source.

Now in (5.4, 5.5, 5.6), we will examine the same images as in the previous case, but with the addition of the pansharpening technique from the MatLab software.

Figure 5.4: Images of Red LED in Matlab with levels 10, 50 and 200 of brightness.

Figure 5.5: Images of Green LED in Matlab with levels 10, 50 and 200 of brightness.

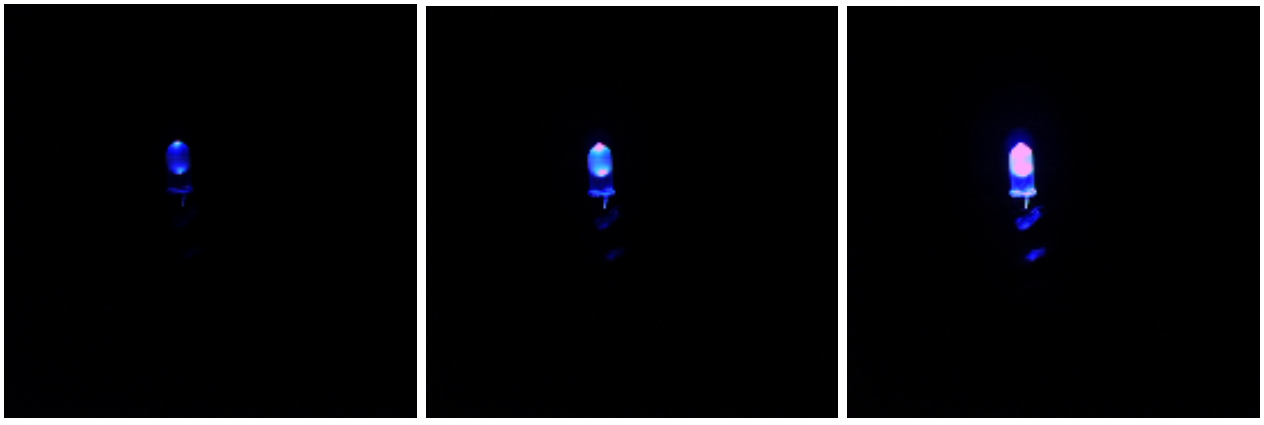

Figure 5.6: Images of Blue LED in Matlab with levels 10, 50 and 200 of brightness.

It is evident that there are considerable discrepancies in the outcomes of the two pansharpening techniques, despite the initial images being identical. The MatLab technique allows us to observe that the black background of the images has remained unchanged, with no alterations in colour. This permits the LED of each image to be observed with clarity. In contrast to the SNAP technique, the diodes are observed in each image with considerably less brightness, particularly when their brightness is 10. This is evident in the case of the green LED in its entirety. It can be observed that, for a brightness of 10, light is not visible to the naked eye, and that, for a brightness of 50, it is barely discernible. At a brightness of 200, a point of light is discernible, although it is not sufficiently sharp to permit identification of the light source.

Concurrently, the source of the red LED is discernible at brightness levels of 50 and 200. Furthermore, it can be observed that the brightness between 50 and 200 does not differ significantly, and that the sensor with pansharpening reproduces them with remarkable fidelity. This is a crucial finding, as it indicates that if our camera is capable of accurately identifying and capturing information across a similar range of brightnesses, with minimal data errors, we can identify an optimal brightness range for the diode. This would ensure that the diode conducts sufficient current to be distinguishable by the camera, while simultaneously ensuring that the current is minimal, thus reducing energy consumption. This would result in an optimal balance that would enhance the profitability of optical communications.

Similarly, it can be observed that the blue diode is the most distinguishable from the background, with the other two diodes appearing less distinct. As illustrated in the images, the blue diode is the sole component of the three that exhibits the reflection previously observed in the preceding results. This may be attributed to the fact that the SNAP software is capable of capturing a greater quantity of information for each pixel, thereby enabling it to detect and process these reflections despite the presence of background noise.

Additionally, it is noteworthy that the diode's interior colour varies depending on the brightness in the different images. This phenomenon may be attributed to a number of potential causes, including the displacement of the emission peak due to an increase in the temperature of the LED, or even an error in the program itself when processing the image within the system.

6 Conclusions

Como conclusiones finales podemos afirmar que ha sido posible cumplir el objetivo principal establecido en el trabajo, que era el de demostrar que las imágenes tomadas por el sensor óptico de la cámara multiespectral podían ser mejoradas a partir de la técnica de pansharpening. Gracias a esta mejora, se facilita la correcta y eficiente comunicación a partir de la luz visble en OCC, lo que permite una conexión inalámbrica diferente con ciertas ventajas con respecto a sus rivales, que serían por un lado el Bluetooth y por el otro el WIFI. De esta manera, se recalca la importancia de estudiar nuevas e innovadoras formas de poder transmitir información de forma rápida y a bajo coste que puedan utilizarse cada vez más en diferentes áreas del conocimiento.

This study has enabled an understanding of the functioning of OCC technology and the means of enhancing it, thereby rendering it a more cost-effective and efficient alternative in certain sectors than competing technologies such as Bluetooth or WiFi. The pansharpening technique has been observed to be highly beneficial in enhancing the quality of images captured by the multispectral camera sensor. It enables the extraction of the detail of the panchromatic band and the colour of the multispectral band, which are then combined to create a final image with the characteristics of each band.

It has been observed that the MatLab and SNAP software employ disparate methodologies for image acquisition and pansharpening. This discrepancy can be attributed to the inherent design of these systems, which are typically employed to analyse images of disparate characteristics. In the case of SNAP, it is used with satellite images that can have spatial resolutions of the order of metres to the order of hundreds of kilometres. This can be affected by including images with spatial resolutions of less than a metre. In the case of the images processed with SNAP, they were initially observed to exhibit considerably more noise than in the case of MatLab. In MatLab, only the light source and a black background were observed, while in SNAP, there were numerous points of noise in the background. However, subsequent application of the pansharpening technique enabled the observation of images in which, despite the presence of background colours other than black, the contrast between the background and the diode was clearly discernible, and in the majority of cases, the silhouette of the LED could be discerned.

The necessity to examine the manner in which images captured by multispectral cameras from disparate systems were processed arose from the objective of comparing the outcomes and determining which software was more effective or superior to the others. In the case of MatLab, it was initially believed that it would be more effective because the initial image was more closely aligned with the real image observed when it was taken, with minimal background noise, and its final image was a version similar to the initial one but enhanced, with no noise and minimal reflection in the images. However, upon examination of the final SNAP images, it became evident that the diodes were, in almost all cases, perfectly visible, even exhibiting greater brightness than in MatLab. To illustrate, in the case previously discussed in the RESULTS section, the green LED at different brightness levels in SNAP

provided greater detail of the source silhouette than in MatLab. This was because in MatLab it was not possible to discern whether it was a diode, as only a faint light source was visible in a very small fraction of the image.

Similarly, it was observed that whether the current was continuous or variable had a significant effect on the initial and final images. For the case shown in the **METHODOLOGY**, where the current passing through the light sources was constant, it was observed that for the SNAP, the light sources presented distortions in the initial and final images, while for the MatLab case this did not occur, but the final images hardly showed any major changes apart from a certain increase in brightness.

Concurrently, this investigation has revealed that an elevation in the temperature of the source, resulting from an increase in the current passing through it, has led to a shift in the emission peak of each diode. This has demonstrated the feasibility of applying a theoretical approach to the effects of temperature on LEDs in a practical setting. This was made possible by the use of a multispectral camera, which would have been impractical with a conventional camera. Consequently, had a hyperspectral camera been available, it is conceivable that the fluctuations in the emission peak could not only have been observed for each of the LEDs, but also that several shifts in more than one band might have been discernible.

It is evident that OCC must continue to evolve if it is to establish itself as a pioneering VLC in scientific progress. However, this progress is being made rapidly thanks to the significant efforts being made by the scientific community that focuses on optical communications, which is gradually making it applicable to more fields of knowledge.

References

[1] Daniel Moreno, Julio Rufo, Victor Guerra, Jose Rabadan, and Rafael Perez-Jimenez. Effect of temperature on channel compensation in optical camera communication. *Electronics*, 10(3):262, 2021.

[2] Syed Muslim Jameel, Abdul Rehman Gilal, Syed Sajjad Hussain Rizvi, Mobashar Rehman, and Manzoor Ahmed Hashmani. Practical implications and challenges of multispectral image analysis. In *2020 3rd International Conference on Computing, Mathematics and Engineering Technologies (iCoMET)*, pages 1–5, 2020.

[3] Rizwan Qureshi, Muhammad Uzair, Khurram Khurshid, and Hong Yan. Hyperspectral document image processing: Applications, challenges and future prospects. *Pattern Recognition*, 90:12–22, 2019.

[4] Lloyd Windrim, Angus J. Carnegie, Murray Webster, and Mitch Bryson. Tree detection and health monitoring in multispectral aerial imagery and photogrammetric pointclouds using machine learning. *IEEE Journal of Selected Topics in Applied Earth Observations and Remote Sensing*, 13:2554–2572, 2020.

[5] Rahul T. S., J. Brema Karunya, and G. Jims John Wessley. A novel remote sensing based approach to estimate the water quality index using sentinel-2 multispectral data. In *2022 International Conference on Smart Technologies and Systems for Next Generation Computing (ICSTSN)*, pages 1–4, 2022.

[6] J. Marcello, D. Rodríguez-Esparragón, and D. Moreno. Comparison of land cover maps using high resolution multispectral and hyperspectral imagery. In *IGARSS 2018 - 2018 IEEE International Geoscience and Remote Sensing Symposium*, pages 7312–7315, 2018.

[7] H.G. Wilson, B. Boots, and A.A. Millward. A comparison of hierarchical and partitional clustering techniques for multispectral image classification. In *IEEE International Geoscience and Remote Sensing Symposium*, volume 3, pages 1624–1626 vol.3, 2002.

[8] T. Blaschke. Object based image analysis for remote sensing. *ISPRS Journal of Photogrammetry and Remote Sensing*, 65(1):2–16, 2010.

[9] Victor-Emil Neagoe and Vlad Chirila-Berbentea. A novel approach for semi-supervised classification of remote sensing images using a clustering-based selection of training data according to their GMM responsibilities. In *2017 IEEE International Geoscience and Remote Sensing Symposium (IGARSS)*, pages 4730–4733, 2017.

[10] M W Vannier, R L Butterfield, D Jordan, W A Murphy, R G Levitt, and M Gado. Multispectral analysis of magnetic resonance images. *Radiology*, 154:221–224, 1 1985.

[11] T. Taxt and A. Lundervold. Multispectral analysis of the brain in magnetic resonance imaging. In *Proceedings of IEEE Workshop on Biomedical Image Analysis*, pages 33–42, 1994.

[12] F. Meriaudeau, V. Paquit, N. Walter, J. Price, and K. Tobin. 3D and multispectral imaging for subcutaneous veins detection. In *2009 16th IEEE International Conference on Image Processing (ICIP)*, pages 2857–2860, 2009.

[13] Pinky A. Bautista and Yukako Yagi. Digital staining for histopathology multispectral images by the combined application of spectral enhancement and spectral transformation. In *2011 Annual International Conference of the IEEE Engineering in Medicine and Biology Society*, pages 8013–8016, 2011.

[14] Naoki. Kobayashi, Hiroyuki. Suzuki, Masahiro Ishikawa, Takashi Obi, Takaya Ichimura, Hiroto Yanagisawa, Tetsuya Tsuchida, and Atsushi Sasaki. Telepathology support system with gross specimen image using high resolution 4K multispectral camera. In *2020 42nd Annual International Conference of the IEEE Engineering in Medicine Biology Society (EMBC)*, pages 1388–1381, 2020.

[15] Dhanushka Chamara Liyanage, Mart Tamre, and Robert Hudjakov. Hyperspectral/multispectral imaging methods for quality control. In *Handbook of Research on New Investigations in Artificial Life, AI, and Machine Learning*, pages 438–461. IGI Global, 2022.

[16] Isabel Moscol, Gleen Peltroche, Victor Ruesta, and Jose Sanchez. Prediction of the main quality parameters of fishmeal to automate the drying process using hyperspectral imaging and artificial neural networks. In *2020 IEEE Engineering International Research Conference (EIRCON)*, pages 1–4, 2020.

[17] Florian Gruber, Philipp Wollmann, Benjamin Schumm, Wulf Grählert, and Stefan Kaskel. Quality control of slot-die coated aluminum oxide layers for battery applications using hyperspectral imaging. *Journal of Imaging*, 2(2), 2016.

[18] Swati Singh, Praveen Pandey, Mohd. Saleem Khan, and Manoj Semwal. Multi-temporal high resolution unmanned aerial vehicle (UAV) multispectral imaging for menthol mint crop monitoring. In *2021 6th International Conference for Convergence in Technology (I2CT)*, pages 1–4, 2021.

[19] Sourabhi Debnath, Manoranjan Paul, D. M. Motiur Rahaman, Tanmoy Debnath, Lihong Zheng, Tintu Baby, Leigh M. Schmidtke, and Suzy Y. Rogiers. Identifying individual nutrient deficiencies of grapevine leaves using hyperspectral imaging. *Remote Sensing*, 13(16), 2021.

[20] Yue Wu, Xican Li, Qing Zhang, Xiaozhen Zhou, Hongbin Qiu, and Panpan Wang. Recognition of spider mite infestations in jujube trees based on spectral-spatial clustering of hyperspectral images from UAVs. *Frontiers in plant science*, 14:1078676, 2023.

[21] Sardor Hazratov and Gokhan Bilgin. Mitosis detection in multispectral histopathological images with deep learning. In *2019 Medical Technologies Congress (TIPTEKNO)*, pages 1–4, 2019.

[22] Akin Ozdemir and Kemal Polat. Deep learning applications for hyperspectral imaging: A systematic review. *Journal of the Institute of Electronics and Computer*, 2:39–56, 2020.

[23] Julio Torres-Tello and Seok-Bum Ko. Identifying useful features in multispectral images with deep learning for optimizing wheat yield prediction. In *2021 IEEE International Symposium on Circuits and Systems (ISCAS)*, pages 1–5, 2021.

[24] Daniel Moreno, Julio Rufo, Victor Guerra, Jose Rabadan, and Rafael Perez-Jimenez. Optical multispectral camera communications using led spectral emission variations. *IEEE photonics technology letters*, 33(12):591–594, 2021.

[25] Yatendra Pal Varshni. Temperature dependence of the energy gap in semiconductors. *physica*, 34(1):149–154, 1967.

[26] Daniel Moreno, Victor Guerra, Julio Rufo, Jose Rabadan, and Rafael Perez-Jimenez. Multispectral optical camera communication links based on spectral signature multiplexing. *IET Optoelectronics*, 17(4):91–100, 2023.

[27] Muna E Raypah, Mutharasu Devarajan, and Fauziah Sulaiman. Influence of injection current and ambient temperature on intensity and wavelength of low-power smd led. In *2016 Ieee 37th international electronics manufacturing technology (Iemt) & 18th electronics materials and packaging (Emap) conference*, pages 1–6. IEEE, 2016.

[28] Muna E Raypah, Bashiru K Sodipo, Mutharasu Devarajan, and Fauziah Sulaiman. Estimation of luminous flux and luminous efficacy of low-power smd led as a function of injection current and ambient temperature. *IEEE Transactions on Electron Devices*, 63(7):2790–2795, 2016.

[29] ChuanZhen Zhao, Rong Zhang, Bin Liu, DeYi Fu, Hui Chen, Ming Li, ZiLi Xie, XiangQian Xiu, ShuLin Gu, and YouDou Zheng. The temperature dependence of optical properties of ingan alloys. *Science China Physics, Mechanics and Astronomy*, 55:396–399, 2012.

[30] Jeong Park and Chin C Lee. An electrical model with junction temperature for light-emitting diodes and the impact on conversion efficiency. *IEEE Electron Device Letters*, 26(5):308–310, 2005.

[31] Anna Andonova, Rumen Yordanov, and Irena Yordanova. Thermal stability analysis of power led during aging. In *Proceedings of the 2011 34th International Spring Seminar on Electronics Technology (ISSE)*, pages 274–278. IEEE, 2011.

[32] Chih-Ju Chan, Feng-Mao Hsu, Yen-Fu Su, and Kuo-Ning Chiang. Study on current and junction temperature stress aging effect for accelerated aging test of light emitting diodes. In *2016 International Conference on Electronics Packaging (ICEP)*, pages 62–65. IEEE, 2016.

[33] V Becirovic, V Helac, B Arslanagic, and H Samic. Effects on leds during the accelerated ageing test. In *2019 18th International Symposium INFOTEH-JAHORINA (INFOTEH)*, pages 1–6. IEEE, 2019.

[34] Gemine Vivone, Mauro Dalla Mura, Andrea Garzelli, Rocco Restaino, Giuseppe Scarpa, Magnus O Ulfarsson, Luciano Alparone, and Jocelyn Chanussot. A new benchmark based on recent advances in multispectral pansharpening: Revisiting pansharpening with classical and emerging pansharpening methods. *IEEE Geoscience and Remote Sensing Magazine*, 9(1):53–81, 2020.

[35] Sinan Jasim Hadi, Mustafa Tombul, Sinan Q. Salih, Nadhir Al-Ansari, and Zaher Mundher Yaseen. The capacity of the hybridizing wavelet transformation approach with data-driven models for modeling monthly-scale streamflow. *IEEE Access*, 8:101993–102006, 2020.

Appendix A

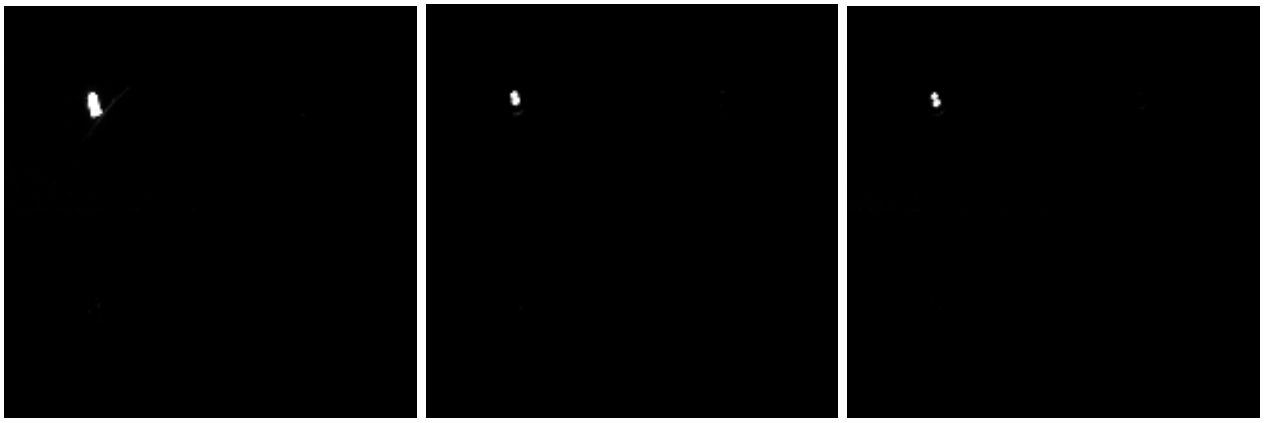

Figure 6.1: MS post-USWT images of Red LED.

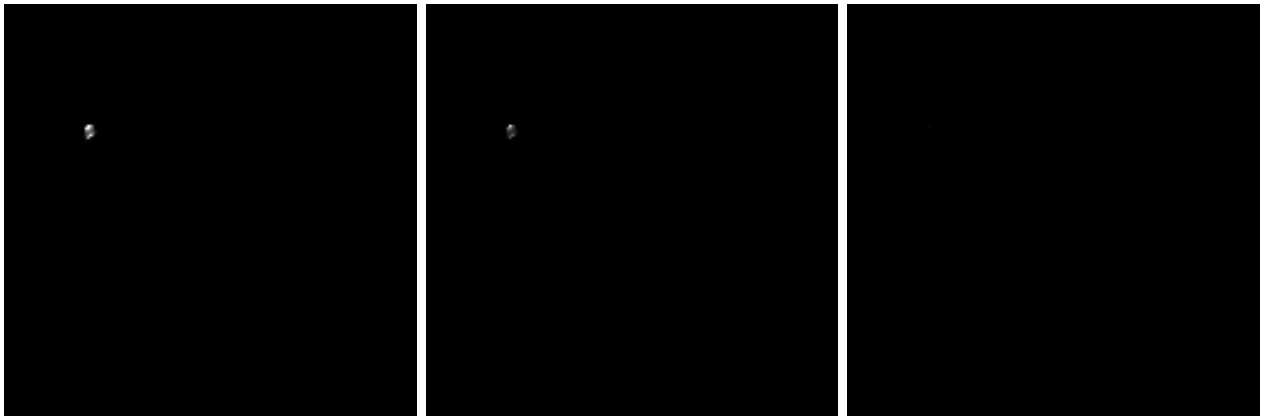

Figure 6.2: MS post-USWT images of Green LED.

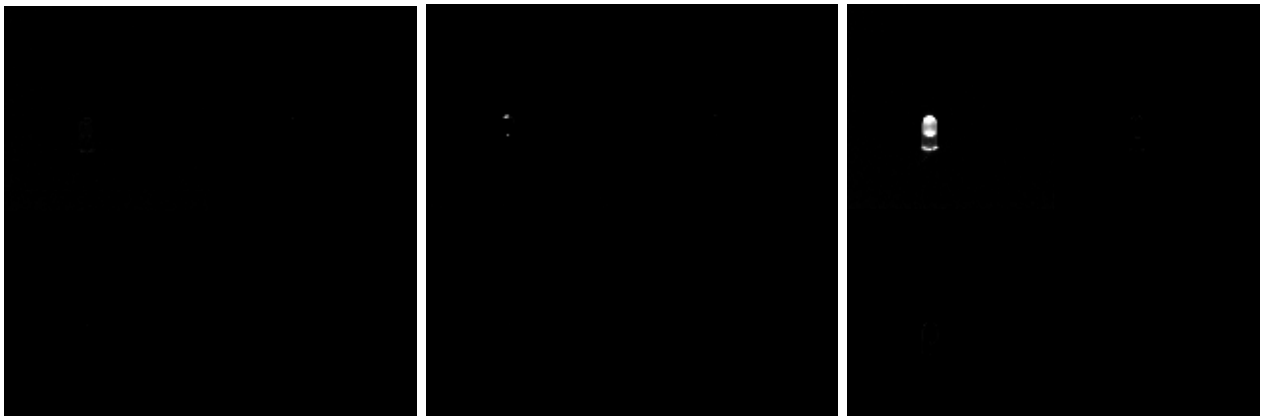

Figure 6.3: MS post-USWT images of Blue LED.

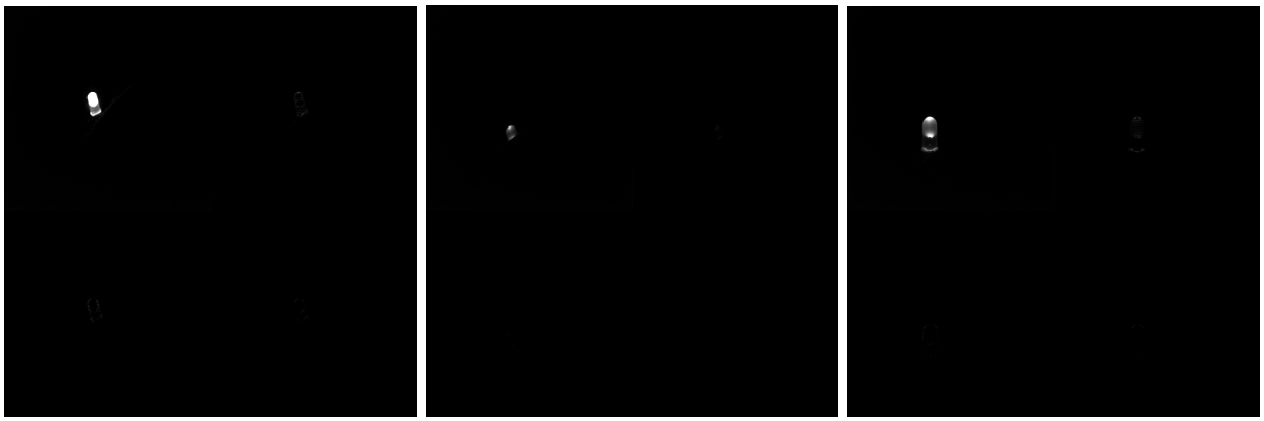

Figure 6.4: UDTW PAN images of Red, Green and Blue LEDs.

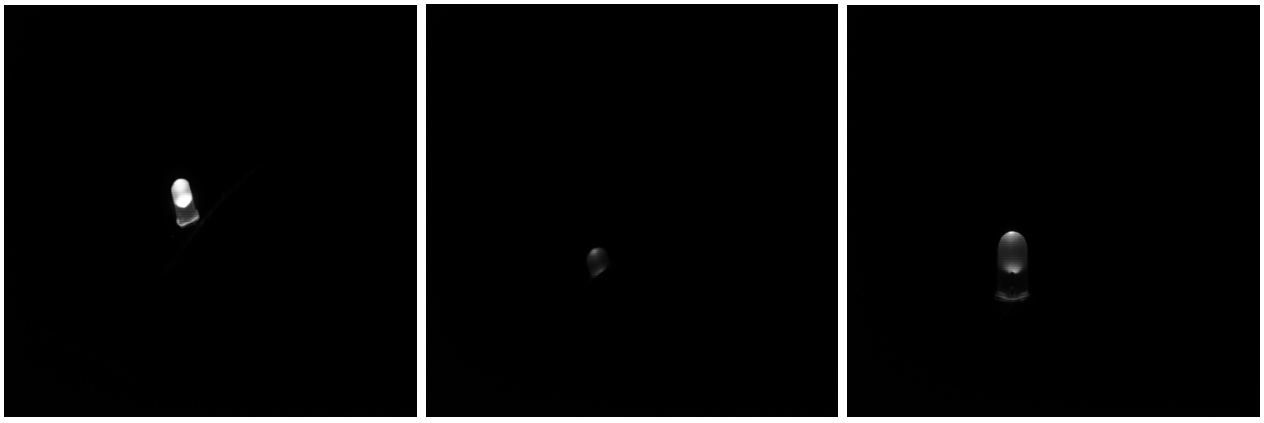

Figure 6.5: Decoded-UDTW PAN images of Red, Green and Blue LEDs.